DESIGN OF A HIGH SENSITIVITY SENSOR FOR METHANE GAS DETECTION

Project report submitted
in partial fulfilment of the requirement for the degree of

Bachelor of Technology

By

Anupal Deuri Bharali (190610026007)
Bhupali Sarma (200610026013)
Ritul Paul (200612726015)
Tushar Nath (200610026060)

Under the guidance of

DR. BIJOY GOSWAMI
(Assistant Professor)
&
MR. NIRANJAN JYOTI BORAH
(Assistant Professor)

DEPARTMENT OF ELECTRONICS & TELECOMMUNICATION ENGINEERING
ASSAM ENGINEERING COLLEGE
JALUKBARI- 781013, GUWAHATI

June 2024

CERTIFICATE

This is to certify that the report entitled "Design of a High Sensitivity Sensor for Methane Gas Detection" submitted by Anupal Deuri Bharali, Bhupali Sarma, Ritul Paul and Tushar Nath in the partial fulfilment of the requirements for the award of Bachelor of Technology degree in Electronics & Telecommunication Engineering at Assam Engineering College, Jalukbari, Guwahati is an authentic work carried out by them under my supervision and guidance. To the best of my knowledge, the matter embodied in the project has not been submitted to any other University/Institute for the award of any Degree or Diploma.

Signature of Supervisors

_____

Dr. Bijoy Goswami

_____

Niranjan Jyoti Borah

STATEMENT OF ORIGINALITY

We declare that this written submission represents our ideas in our own words and where others' ideas or words have been included, we have adequately cited and referenced the original sources. We acknowledge that the work presented in this project report has been completed in accordance with the guidelines and regulations set forth by Assam Engineering College. We take full responsibility for the content and accuracy of the information presented herein. We also declare that we have adhered to all principles of academic honesty and integrity and have not misrepresented or fabricated or falsified any idea/data/fact/source in our submission. We understand that any violation of the above will be cause for disciplinary action by the Institute and can also evoke penal action from the sources.

Name	Roll Number	Signature
1. Anupal Deuri Bharali	190610026007	
2. Bhupali Sarma	200610026013	
3. Ritul Paul	200612726015	
4. Tushar Nath	200610026060	

ACKNOWLEDGMENTS

We would like to express our sincere thanks to the Head of the Electronics and Telecommunication Engineering (ETE) Department, Dr. Navajit Saikia at Assam Engineering College for his support and guidance throughout our academic journey. We are grateful for his role in fostering a conducive learning environment in the department. We extend our heartfelt appreciation to Dr. Bijoy Goswami, Assistant Professor, Department of Electronics and Telecommunication Engineering, Assam Engineering College, for his invaluable contributions and visionary mentorship. His unwavering support, technical expertise and expert insights have been pivotal in guiding us through the complexities of the project and broadening our perspectives. In addition, we would like to extend a heartfelt gratitude to our co-guide Mr. Niranjan Jyoti Borah for his support. Also, to our parents, their unswerving love, encouragement, and belief in our abilities have been the cornerstone of our accomplishments. They have been our constant source of motivation and support. Finally, we extend our sincere thanks to all our teammates who collaborated tirelessly throughout the project's execution. Each team member's unique skills and contributions have added immense value to the project, and we are truly grateful for their immense support.

Anupal Deuri Bharali (190610026007)
Bhupali Sarma (200610026013)
Ritul Paul (200612726015)
Tushar Nath (200610026060)

ABSTRACT

This project seeks to develop a creative response to the growing concerns about safety and environmental wellbeing, notably about potential methane gas leaks in CNG automobiles and gas stations. The primary goal is to develop a highly sensitive and specific methane gas sensor to address this urgent issue. The absence of effective sensors has created a worrying gap in detecting leaks, posing risks to human life and the surrounding ecosystems.

This project focuses on creating a methane gas sensor with average sensitivity and precision. The sensor's unique design involves combining n type substrate of uniform doping with Boron-Nitride layer which has methane-reactive properties. This combination enhances the sensor's ability to interact with methane gas molecules effectively. By carefully orchestrating these components, the sensor's performance in detecting methane gas is expected to surpass existing technologies.

Leveraging the advanced resources of SilvaCo., the sensor's intricate design and functionality will undergo thorough simulation and refinement. This meticulous process aims to perfect the sensor's features before it becomes a tangible product. Once developed, integrating this sensor into CNG vehicles and gas stations will enable real-time monitoring of methane gas levels. This proactive approach has the potential to significantly reduce the risks of accidents, explosions, and environmental damage caused by unnoticed methane leaks.

The envisioned outcome of this project is a robust sensor system that not only detects methane gas leaks promptly but also demonstrates its practicality for widespread use. Successfully implementing this sensor could revolutionize safety standards in CNG transportation and storage, leading to a safer, cleaner, and more sustainable energy landscape. By addressing this critical technology gap, this initiative represents a significant step toward a safer and more ecologically balanced world. Currently in the pre-implementation phase, the project aims to turn these ambitions into concrete realities in the upcoming stages.

LIST OF TABLES

LIST OF FIGURES

CONTENTS

CHAPTER 1
INTRODUCTION

1.1 Introduction

The project has gone covert to develop a high-performance sensor using junctionless TFETs for methane gas detection in CNG vehicles. The project explores the design, simulation and optimization of this revolutionary sensor device using the capabilities of SilvaCo. TCAD (Technical Computer Aided Design) software. In this chapter we focus on various topics which form the base of the project, and henceforth motivate us to arrive at the desired results of the project. This chapter has been divided into several sections as discussed below. Firstly, we provide a brief introduction to the area of work and provide insights to various phenomena involved in the background of developing this project.

1.2 History and development of semiconductors

A semiconductor is a material that has an electrical conductivity value falling between that of a conductor, such as copper, and an insulator, such as glass. Its resistivity generally falls as its temperature rises; metals behave in the opposite way. In many cases their conducting properties may be altered in useful ways by introducing impurities (‘doping’) into the crystal structure. When two differently doped regions exist in the same crystal, a semiconductor junction is created. The behaviour of charge carriers, which include electrons, ions, and electron holes, at these junctions is the basis of diodes, transistors, and most modern electronics. Some examples of semiconductors are silicon, germanium, gallium arsenide, and elements near the so-called "metalloid staircase" on the periodic table. After silicon, gallium arsenide is the second-most common semiconductor and is used in laser diodes, solar cells, microwave-frequency integrated circuits, and others. Silicon is a critical element for fabricating most electronic circuits.

The history of semiconductors and their development traces back to the early 20th century. Here's a brief overview:

1. Early Discoveries (1833-1904):
    - In 1833, Michael Faraday conducted experiments on the electrical properties of silver sulphide, a semiconductor material.
    - In 1904, Japanese scientist Jagadish Chandra Bose demonstrated the semiconductor properties of galena (lead sulphide) crystals and their ability to detect and generate radio waves.

2. Germanium and the Point-Contact Transistor (1930s-1940s):
    - In 1931, German physicists Karl Seeger and Paul Harteck demonstrated the semiconductor properties of silicon and germanium.
    - In 1947, John Bardeen, Walter Brattain, and William Shockley at Bell Labs invented the point-contact transistor, the first transistor made from germanium.

3. The Silicon Revolution (1950s-1960s):
    - In 1954, Gordon Teal at Texas Instruments developed the first commercial silicon transistor.
    - In 1958, Jack Kilby at Texas Instruments invented the integrated circuit (IC), which combined multiple transistors on a single semiconductor chip.
    - In 1959, Robert Noyce at Fairchild Semiconductor independently invented the integrated circuit using a different manufacturing process.
4. Microprocessor and Memory Development (1960s-1970s):
    - In 1961, the first semiconductor memory chip was introduced by Fairchild Semiconductor.
    - In 1971, Intel introduced the first commercial microprocessor, the Intel 4004, which paved the way for personal computers and numerous digital devices.
5. Scaling and Miniaturization (1970s-present):
    - The semiconductor industry has continued to follow Moore's Law, doubling the number of transistors on a chip approximately every two years, leading to smaller, more powerful, and more energy-efficient devices.
    - Advances in lithography, materials science, and manufacturing techniques have enabled the scaling down of transistor sizes and the integration of billions of transistors on a single chip.
6. Modern Applications (1990s-present):
    - Semiconductors are now found in a wide range of applications, including computers, smartphones, consumer electronics, automotive systems, medical devices, and various other industries.
    - New semiconductor materials and technologies, such as gallium arsenide, silicon-germanium, and more recently, graphene and other 2D materials, have been explored for specialized applications.

1.3 Introduction to the area of work

The emphasis on sustainable energy, particularly the increased use of Compressed Natural Gas (CNG) in transportation, has highlighted the need for effective monitoring systems. Detecting methane, a crucial component of natural gas, is essential for ensuring the safe use of CNG. The design of a high-sensitivity methane sensor for CNG vehicles and stations is a crucial effort focused on improving safety, preventing hazards, and sustaining the viability of CNG as a clean energy solution. The endeavour addresses challenges in detecting odourless and colourless methane, emphasizing the importance of a highly sensitive sensor for timely responses to potential leaks in CNG environments.

The primary goal of this project is to develop a Junctionless Field-Effect Transistor based sensor used to detect methane gas to achieve high sensitivity, accuracy, and efficiency in the detection process of the gas which is otherwise difficult to detect due to it being colourless and odourless. The unique properties of Junctionless FETs, which rely on quantum tunnelling for their operation, make them well-suited for gas sensing applications. In the context of methane detection, the specific goals include high sensitivity which comes when current ON/OFF ratio of the device is low, high selectivity ensuring minimal interference from other gases or environmental factors, low power consumption, reliability and stability.

1.4 Brief present-day scenario with regard to the work area

Research and development in methane sensing using Junctionless Field-Effect Transistors (JLFETs) are advancing. TFETs are gaining attention for their potential in providing high sensitivity and low power consumption in gas sensing applications, particularly for methane detection. The focus is on improving sensor performance through the exploration of new materials and fabrication techniques. Integration into Internet of Things (IoT) devices for real-time monitoring and potential deployment in industrial settings, such as those involving natural gas and CNG, are few more notable trends. Challenges related to calibration and mass production are some areas of exploration.

1.5 Motivation of doing the project

The motivation behind designing a Junctionless TFET-based sensor for methane detection stems from the desire to leverage the unique properties of Junctionless FETs, such as high sensitivity, low power consumption, and miniaturization, to create advanced and efficient methane sensing devices for various applications, including environmental monitoring and industrial safety.

1.6 Objective of the work

Objective 1: To understand the sensitivity of a single gate TFET structure

• Design of a single gate TFET in SilvaCo. TCAD software and to investigate its

behaviour in terms of subthreshold swing, $I_{ON/OFF}$ ratio and transconductance.

• Plots exhibiting VI-transfer characteristics, voltage, band to band tunnelling, and electric field of the TFET device.

• Usage of different metals- Al, Mo, Pt, Au for construction of gate structure.

Objective 2: To understand the sensitivity of a dual gate TFET structure

• Design of a dual gate TFET in SilvaCo. TCAD software by integrating gate structures on both sides of the Si-substrate and to investigate its behaviour in terms

of subthreshold swing, $I_{ON/OFF}$ ratio and transconductance.

• Plots exhibiting VI-Transfer characteristics, voltage, band to band tunnelling, and electric field of the TFET device.

• Usage of different metals- Al, Mo, Pt, Au for construction of gate structure.

Objective 3: To understand the sensitivity of a junctionless TFET structure

• Design and simulation of a junctionless dual-gate TFET in Silvaco TCAD to explore its performance for sensor applications by analyzing VI characteristics.

• Investigation of the electric field distribution, potential, and band-to-band tunnelling effects in the junctionless dual-gate TFET structure.

• Validate the junctionless dual-gate TFET's suitability for sensor applications through comparative analysis with traditional FET designs under varying conditions.

1.7 Target Specifications

Designing target specifications for a junctionless TFET based methane gas sensor using Silvaco TCAD software involves considering parameters specific to Junctionless TFET device design and methane gas detection. Here are the target specifications defined for this project:

1. Device Geometry and Material Properties:

- Defining the dimensions of the Junctionless TFET sensor structure, including channel length, channel thickness, and gate length.
- Specifying the material properties of the semiconductor layers, such as bandgap, electron affinity, and effective masses.

2. Operating Conditions:

- Setting the operating temperature for the simulation, considering the expected environmental conditions.
- Defining the biasing conditions, including drain-source voltage and gate voltage, for methane gas detection.

3. Electrical Characteristics:

- Targetting Junctionless TFET characteristics such as subthreshold swing, on-state current, and off-state leakage current.
- Optimizing the Junctionless TFET design to achieve low-power operation and high sensitivity to methane gas.

6. Simulation Output:

- Defining the desired output parameters, such as electric field, potential, drain current, transfer characteristics, BTBT, and sensitivity to methane gas concentration.
- Specifying the simulation time and convergence criteria for accurate results.

8. Integration with Experimental Data:

- Comparing simulated Junctionless TFET sensor responses with experimental measurements under various methane gas concentrations.

9. Optimization Goals:

- Setting optimization goals for improving sensor performance, such as maximizing sensitivity, minimizing power consumption, or enhancing selectivity to methane gas.
- Exploring design parameters (e.g., channel length, gate material) to optimize the Junctionless TFET sensor for methane gas detection.

10. Visualization and Analysis Tools:

- Utilizing visualization and analysis tools within Silvaco TCAD for interpreting simulation results, including 2D/3D plots, current-voltage characteristics, and charge distribution profiles.
- Defining criteria for evaluating the Junctionless TFET sensor's performance and effectiveness in detecting methane gas.

By defining these target specifications within Silvaco TCAD software, you can guide the simulation and design process to develop a junctionless TFET-based methane gas sensor optimized for performance, sensitivity, and reliability.

1.8 Organization of the report

The report is organised in different chapters as follows: Chapter 1 gives a brief introduction about the area of work. This chapter contains present day scenario, motivation to do the work, objective of the project, target specification and importance of the result. Chapter 2 discuss about the literature review. This chapter contains information regarding the project area from various platforms and previous works. Chapter 3 discusses about the devices that are to be used for the final design, the research methodology adopted and tools used for the completion of the work. Chapter 4 contains briefly about the experimental designs that were initially taken up during the course of this project to build the sensor. Chapter 5 describes the various detailed graphs obtained as a result of the project work. Chapter 6 contains the results, conclusion with its future scope.

CHAPTER 2
LITERATURE REVIEW

2.1 Introduction

Methane gas has a substantial influence on human health and environmental safety, making its detection crucial. Strong greenhouse gas methane creates a significant risk of explosion in enclosed areas and has a significant role in global warming. Thus, it is crucial to build sensitive and trustworthy methane gas sensors. This chapter on literature study explores the basic and advanced ideas related to our research, which is to construct a junctionless Tunnel Field-Effect Transistor (TFET)-based sensor for the detection of methane gas.

We examine the basic ideas behind TFETs, emphasizing how their distinct operating mechanisms set them apart from traditional MOSFETs. A thorough analysis of their band-to-band tunnelling method, which has clear benefits in low-power and high-sensitivity applications, is part of this. The idea of junctionless TFETs is then introduced, which is a novel technique that simplifies fabrication procedures and may improve performance metrics like sensitivity and scalability by doing away with internal junctions in the device.

Simultaneously, an examination is conducted into the incorporation of TFETs into biosensor technology, highlighting their suitability for the detection of diverse biological and chemical contaminants. This section highlights the potential of TFET-based biosensors to attain high levels of detection precision at low power consumption by offering insights into their sensitivity analysis.

The following sections describe the material compositions, performance characteristics, and operational principles of methane gas sensors. Focus is specifically on the gas sensing capabilities of boron nitride, a material that is well-known for its exceptional electrical properties, huge surface area, and high thermal stability. To better understand how boron nitride can improve sensor performance, particularly when it comes to methane detection, its integration into sensor technology is assessed.

A thorough analysis of the most recent TFET-based biosensors, especially those intended for gas detection, and their corresponding performance measures are also included in this chapter.

By analyzing sensitivity, selectivity, response time, and operational stability, this offers a comprehensive knowledge of the state of technology today and the achievements that have been made thus far.

The present literature evaluation provides a strong basis for our research endeavour by consolidating essential ideas and advancements in the domains of junctionless TFETs, biosensors, methane gas detection, and TFETs. It emphasizes how important our suggested sensor technology is and how much it can advance the field of gas sensing.

2.2 Study of Tunnel Effect Field Transistor

Nardi et al. [8] provides a comprehensive review of junction-less transistors (JLTs), emphasizing their simplified fabrication process and suitability for nanoscale applications. By eliminating the need for junctions, JLTs offer a significant advantage in manufacturing, particularly for devices smaller than 10 nm. The paper categorizes JLTs into depletion-based and tunnel-based types and further classifies them by geometrical shape, material composition, and gate structure. Key performance metrics such as Drain-Induced Barrier Lowering (DIBL), subthreshold swing (SS), and Ion/Ioff ratios are thoroughly discussed. Advanced structures like Gate-All-Around (GAA) and FinFET JLTs are highlighted for their superior performance metrics, including high Ion/Ioff ratios and minimal short channel effects. The impact of different materials, including silicon and germanium, on JLT performance is analyzed, with strain technology identified as a method to enhance device characteristics. The review underscores the technological versatility of JLTs, indicating their potential for further advancements through material innovation and refined fabrication techniques. This study lays a robust foundation for understanding JLT technology's current state and future potential, particularly in optimizing DIBL and SS values for enhanced performance.

Lei Yao et al. [12] explores the design, simulation, and performance of a junctionless tunnel field-effect transistor. The study aims to address the challenges in scaling down conventional MOSFETs by proposing a junctionless structure that eliminates the need for heavily doped source and drain regions. Using a simulation approach, the paper demonstrates that the JUNCTIONLESS TFET achieves significant improvements in subthreshold swing (SS), Drain-Induced Barrier Lowering (DIBL), and I_{ON}/I_{OFF} ratio compared to traditional TFETs. The JUNCTIONLESS TFET shows potential for low-power applications due to its steep subthreshold slope and reduced short-channel effects. The research also highlights the impact

of device parameters such as gate length, oxide thickness, and channel doping concentration on the performance of the Junctionless TFET. The findings suggest that the Junctionless TFET could be a promising candidate for future low-power and high-performance electronic devices, offering a simplified fabrication process and superior electrostatic control. This study lays a foundation for further exploration and optimization of junctionless transistors in nanoscale applications.

Ghosh et al. [13] proposes and investigates a novel double-gate junctionless tunnel field-effect transistor (JL-TFET). This JL-TFET is a silicon-channel, heavily n-type-doped junctionless field-effect transistor (JLFET) that incorporates two isolated gates with different metal work functions to emulate the behaviour of a tunnel field-effect transistor (TFET). The simulation results demonstrate that the JL-TFET, utilizing a high-k dielectric material (TiO2) with a 20-nm gate length, exhibits excellent performance characteristics. These include a high I_{ON}/I_{OFF} ratio of approximately 6×10^8, a point subthreshold slope (SS) of around 38 mV/decade, and an average SS of about 70 mV/decade at room temperature. The findings suggest that the JL-TFET holds significant promise for switching applications due to its superior performance metrics compared to conventional MOSFETs and other alternatives, thus highlighting its potential for future semiconductor technology developments.

2.3 Study of sensing property of Boron Nitride

Goel et al. [9] discusses recent advancements in ultrathin 2D hexagonal boron nitride (hBN) based gas sensors. It highlights the unique properties of hBN, such as high thermal conductivity and temperature stability, making it promising for high-performance gas sensors. The review focuses on the state-of-the-art advances in hBN devices with a specific emphasis on gas sensors, addressing challenges like poor surface reactivity and low conductivity. It delves into the physics and sensing mechanisms of hBN gas sensors, along with strategies to enhance their performance. The synthesis methods of 2D hBN, including mechanical exfoliation and chemical vapor deposition, are explored. The paper also discusses recent developments in hBN and its heterostructures for gas sensing applications, concluding with a perspective on the challenges faced by hBN-based gas sensing technology for practical implementation.

Jacoud et al. [2] discusses the advancements in 2D hexagonal boron nitride (hBN) for electronic and optoelectronic devices, focusing on gas sensors. It highlights hBN's high thermal conductivity and stability, making it ideal for next-gen gas sensors. The review covers the state-

of-the-art advances in hBN-based devices, emphasizing gas sensors, and explains the physics behind hBN-based gas sensors. It also addresses challenges like poor surface reactivity and low conductivity. The paper elaborates on synthesis methods for large-scale hBN growth and strategies to enhance sensor performance. It discusses the physics and sensing mechanisms for gas detection and recent developments in hBN and its heterostructures for gas sensing applications. The review concludes with insights into the challenges faced by hBN-based gas sensing technology for practical implementation, showcasing hBN's potential for various industrial applications beyond gas sensing.

2.4 Study of Bio sensor

Suriyaprakash. S. et al. [1] discusses the design of a Methane Gas Detector using Internet of Things (IoT). It emphasizes the importance of detecting methane gas, a natural gas that can be harmful and explosive when mixed with air. The system comprises a PIC Microcontroller, methane gas sensor, temperature sensor, LCD display, buzzer, and Wi-Fi module. The IoT integration allows for remote monitoring of gas levels. The device is versatile, suitable for both domestic and industrial applications, with a detection range from 200ppm to 10000 ppm. The system continuously updates gas and temperature data to the microcontroller, displaying it on the LCD and sending it to the cloud via Wi-Fi. The design aims to enhance safety in various sectors like gas industries, garbage management, sewage cleaning, and underground mines. Future improvements could include adding more gas sensors for diverse applications and enhancing reliability with redundant sensors. However, limitations such as data loss in underground areas without internet connectivity and limited wireless range are noted.

Sen et al. [3] discusses a novel biosensor based on dielectric modulation using a Dual Metal Gate Engineered SiGe/Si heterostructure Tunnel Field-Effect Transistor (DM-GE-HTFET). The biosensor design incorporates an extended gate engineering mechanism to enhance sensitivity and efficiency. The SiGe/Si heterostructure enables improved fabrication feasibility. Results indicate a significant increase in ON-state current with higher dielectric constant biomolecules, showcasing a high On-Current Sensitivity (SION) of 7.5×10^9 for $\kappa = 12$. Comparative analysis against other TFET-based biosensors demonstrates the promising performance of the proposed DM-GE-HTFET. The architecture offers a large amount of gate electrostatic control and minimizes off-state current, making it a viable alternative for sensitive biosensing applications. Overall, the study highlights the potential of the DM-GE-HTFET

biosensor as a sensitive and efficient label-free biosensing solution with dual metal gate engineering and dielectric modulation.

Mukhopadhyay et al. [5] evaluates the performance of a Dielectrically Modulated Extended Gate Single Cavity InGaAs/Si HTFET-based biosensor, focusing on non-ideal issues. It compares the sensitivity, ON current, I_{ON}/I_{OFF} ratio, and subthreshold swing of different biosensor structures. The SC-DM-EG HTFET biosensor demonstrates superior performance, offering enhanced sensitivity, robustness, and reduced response time. The study includes 2D numerical simulations using SilvaCo. ATLAS software, highlighting the advantages of III-V heterostructure and extended gate geometry for biosensing applications. Sensitivity analyses for neutral and charged biomolecules with varying dielectric constants are conducted, emphasizing the device's high sensitivity and reliability. The research provides insights into the impact of non-ideal factors like temperature fluctuations and steric hindrance on biosensor performance. Overall, the SC-DM-EG HTFET biosensor emerges as a promising, cost-effective, and efficient solution for label-free biosensing applications.

T.A. et al. [6] delves into the significance and technological advancements of various methane detection sensors essential for mitigating methane emissions, a potent greenhouse gas with a global warming potential 28 times greater than carbon dioxide. It reviews five main sensor types: optical, calorimetric, pyroelectric, semiconducting metal oxide, and electrochemical sensors, discussing their definitions, mechanisms, advantages, and limitations. Notably, optical sensors, utilizing infrared absorption spectroscopy, are highlighted for their non-destructive detection and resistance to electromagnetic interference, though they face challenges like higher costs and interference from other hydrocarbons. Recent advancements in sensor materials and design improvements are covered, aiming to enhance sensitivity, accuracy, and response times. The paper underscores the critical need for ongoing research and development to optimize methane sensor technologies, emphasizing their role in early leak detection and mitigation. Such advancements are vital for reducing methane emissions, thereby protecting the environment and offering significant economic benefits through improved resource management and regulatory compliance.

A. Pope et al. [7] introduces a cost-effective, room-temperature methane sensor utilizing laser-induced graphene (LIG) electrodes in commercial polymer films, with palladium nanoparticles enhancing electrocatalytic activity. The sensor employs a pseudo-solid-state ionic liquid/polyvinylidene fluoride electrolyte for efficient methane electro-oxidation, achieving high sensitivity (0.55 μA/ppm/cm²) and a rapid response time of 40 seconds, enabling sub-ppm methane detection. While offering a promising solution for methane leak detection crucial for environmental protection and industrial safety, the sensor has some demerits. Its performance may be affected by environmental factors such as humidity and temperature variations, potentially compromising reliability and accuracy in diverse conditions. Additionally, the long-term stability and durability of the sensor in real-world applications require further evaluation. Future research should enhance the sensor's robustness against environmental variables, extend its operational lifespan, and conduct extensive field tests to validate its performance in various settings. Integrating the sensor with wireless technologies for remote monitoring and real-time data analysis presents a promising direction for future development, improving its applicability and effectiveness in industrial and environmental monitoring.

Dosi et al. [10] presents a novel methane detection technology that addresses the need for efficient and cost-effective monitoring of methane leaks, which are significant contributors to greenhouse gas emissions. The authors developed an electrochemical sensor using laser-induced graphene (LIG) electrodes embedded in commercial polymer films, enhanced with palladium nanoparticles to boost electrocatalytic activity. The sensor uses a pseudo-solid-state ionic liquid/polyvinylidene fluoride electrolyte, achieving remarkable sensitivity (0.55 μA/ppm/cm²) and a rapid response time (40 seconds) at room temperature. This enables the detection of methane at sub-ppm levels, making it highly effective for identifying minor leaks. The fabrication process involves patterning LIG directly into the films and applying a palladium nanoparticle dispersion, which distributes the catalyst within the porous structure. The sensor's performance was thoroughly evaluated under various methane concentrations and humidity levels, including tests against potential interfering gases. This work demonstrates a significant advancement in methane sensing technology, offering a low-cost, highly sensitive, and fast-response solution for environmental monitoring and industrial safety applications.

R. Narang et al. [11] investigates the performance of a p-n-p-n tunnel field-effect transistor (TFET) biosensor compared to a conventional FET-based sensor. It explores the impact of dielectric constant and charge of biomolecules on the electrical parameters of the TFET biosensor. The study reveals that the TFET biosensor offers advantages over FET-based sensors due to its low leakage current in the absence of biomolecules and high sensitivity to dielectric constant and charge effects. The simulation employs a nonlocal band-to-band tunnelling model and introduces a dielectric constant greater than 1 to represent biomolecules in the nanogap. The research also discusses the sensitivity of the TFET biosensor concerning device parameters, process variability, and process-induced damage. By extending the analytical framework to incorporate biomolecule charge effects, the study provides valuable insights into the potential of TFET-based biosensors for developing highly sensitive label-free biomedical diagnostic tools.

N. Reddy et al. [14] discusses the significance of field-effect transistor (FET) biosensors in detecting biomolecules through physiochemical reactions. FET biosensors offer label-free detection and rapid response, making them valuable in various applications such as medical diagnosis, drug delivery, and environmental monitoring. Different TFET structures like SiNWTFET and DMTFET are explored to enhance sensitivity and performance. The detection mechanism involves analyzing targeted biomolecules and converting physiochemical reactions into measurable electrical signals. The study also delves into double gate structures and hetero compositions to improve biosensor capabilities. Analytical models and device architectures are investigated to optimize biosensor functionality. Overall, the research aims to develop advanced TFET biosensors for future applications with improved performance and ease of fabrication, addressing the growing need for accurate and reliable biosensors in various fields.

S. Datta et al. [15] investigates the performance of Tunnel Field-Effect Transistors (TFETs) by exploring their potential applications and associated challenges. TFETs, characterized by their low subthreshold swing and steep subthreshold slope, hold promise for low-power electronics. However, challenges exist in TFET technology, including fabrication complexities due to the need for ultra-thin materials and precise doping profiles. Material selection is also crucial, with concerns about achieving high-quality interfaces and minimizing leakage currents. Optimization techniques such as bandgap engineering and interface engineering are being explored to address these challenges. Despite these hurdles, TFETs show great potential for

energy-efficient circuits and sensors, with future scope lying in further optimizing device structures and exploring novel materials. Additionally, TFET-based sensors could find applications in various fields such as healthcare, environmental monitoring, and industrial automation, where low-power operation and high sensitivity are paramount. Addressing these challenges and exploring diverse applications will be crucial for realizing the full potential of TFET technology.

M. J. Deen et al. [16] scrutinizes the operational mechanisms and performance metrics of Tunnel Field-Effect Transistors (TFETs). Delving into the underlying physics governing TFET operation, the study elucidates concepts such as band-to-band tunnelling and gate control mechanisms. However, TFET performance can be affected by issues such as ambipolar conduction and process variations, which may limit device scalability and yield. Furthermore, the optimization of TFETs for high-speed operation remains a challenge due to limitations in achieving high carrier velocities. Despite these challenges, TFETs hold promise for applications requiring low-power consumption and steep subthreshold slope. Future research directions include exploring novel device architectures, materials, and fabrication techniques to enhance TFET performance. Additionally, TFET-based sensors could benefit from improvements in sensitivity and selectivity, paving the way for advancements in gas sensing, biomedical diagnostics, and environmental monitoring. Overcoming these challenges and exploring new avenues for TFET research will be crucial for realizing the full potential of this technology.

G. Sberveglieriet al. [17] provides a comprehensive overview of methane detection technologies tailored for environmental monitoring applications. Systematically discussing various sensing principles and methodologies, the study evaluates the performance characteristics, advantages, and limitations of different methane detection technologies. It also explores emerging trends and advancements in methane sensor technology, such as miniaturization, integration with Internet of Things (IoT) platforms, and wireless communication for remote monitoring applications, showcasing their potential to revolutionize environmental monitoring practices. However, challenges exist, including the need for improved sensitivity and selectivity, as well as the development of robust and cost-effective

sensor platforms. Future research directions include the exploration of novel sensing materials and integration with advanced data analytics techniques to enhance sensor performance and reliability. Additionally, the deployment of sensor networks and the development of standardized protocols for data sharing and analysis will be crucial for realizing the full potential of methane detection technologies in environmental monitoring applications.

M. Penzaet al. [18] conducts an exhaustive review of recent advancements in chemical sensor technologies, particularly focusing on their applications in environmental monitoring and homeland security. The study systematically discusses various types of chemical sensors, elucidating their principles of operation, fabrication methods, and performance characteristics. Moreover, it highlights recent developments in sensor materials, nanostructured sensing elements, and sensor integration aimed at enhancing sensitivity, selectivity, and stability. Additionally, the study explores applications of chemical sensors in detecting hazardous gases, volatile organic compounds (VOCs), biological agents, and explosives, emphasizing their critical role in ensuring public safety and environmental protection. However, challenges such as cross-sensitivity, calibration requirements, and environmental robustness need to be addressed to improve sensor performance and reliability further. Future research directions include the development of advanced sensor platforms capable of real-time monitoring, as well as the integration of sensor networks with machine learning algorithms for predictive analytics and decision support.

G. Korotcenkov et al. [19] provides an in-depth exploration of gas sensor technologies, encompassing principles of operation, fabrication methods, and diverse applications. The study systematically discusses various types of gas sensors, elucidating their working principles, fabrication techniques, and performance characteristics. Moreover, it examines factors influencing gas sensor performance and explores strategies for sensor optimization. Furthermore, it discusses emerging trends in gas sensor research, highlighting their potential applications in environmental monitoring, industrial safety, and healthcare sectors. The study also addresses challenges such as sensor drift, cross-sensitivity, and response time, which need to be overcome to enhance sensor performance and reliability further. Future research directions include the development of miniaturized and low-cost sensor platforms, as well as the integration of sensor networks with Internet of Things (IoT) platforms for real-time monitoring and data analytics. Additionally, advancements in sensor materials and fabrication

techniques will play a crucial role in unlocking new applications and improving sensor performance for diverse gas sensing applications.

2.5 Conclusion

The significant data about the project is collected and discussed by us. We conclude that these data are collected through various platforms and various previous works performed by other scientists.

CHAPTER 3

INTRODUCTION TO DIFFERENT FET STRUCTURES AND THEIR APPLICATIONS

3.1 Introduction

This chapter explores the approaches employed in this project. It encompasses details regarding the software utilized, the device parameters selected for structuring, and the various analyses conducted.

3.2 Single Gate TFET Structure:

Designing methane gas sensors necessitates a profound comprehension of the intricacies inherent in single gate Tunnel Field-Effect Transistor (TFET) architectures. Single gate TFETs offer heightened sensitivity crucial for detecting subtle changes in methane concentrations, aligning with the project's goal of precision in gas detection. The inherent low power consumption of single gate TFETs holds significance, enabling the creation of energy-efficient sensors vital for sustainable and environmentally responsible long-term operation. This characteristic is particularly relevant in applications such as CNG vehicles and gas stations.

Moreover, the efficiency of single gate TFETs at low working voltages contributes to optimized power consumption, addressing the project's emphasis on energy efficiency. The high-speed operation of single gate TFETs ensures rapid response times, enhancing the sensor's capability for real-time methane gas detection. Reduced heat generation in single gate TFETs further underscores the project's focus on longevity and reliability, crucial in scenarios demanding consistent and enduring sensor performance.

The material flexibility inherent in single gate TFETs is explored as it offers the potential to optimize material choices, tailoring the sensor design to environmental conditions. The compatibility of single gate TFETs with cutting-edge technologies reinforces the sensor's relevance in the dynamic field of gas detection and electronic components. Lastly, the integration and miniaturization capabilities of single gate TFETs position them as suitable for compact systems, aligning with practical needs in applications like gas stations and CNG vehicles. In essence, comprehending the unique qualities of single gate TFETs is paramount for crafting sophisticated, energy-efficient, and sensitive methane gas sensors tailored for diverse real-world situations.

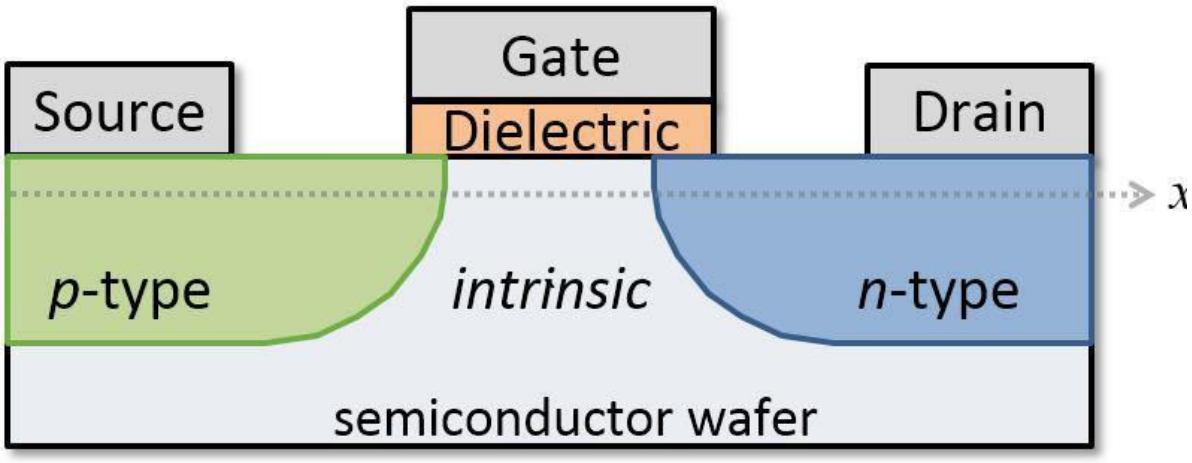

Figure 3.1: A simple single gate TFET Structure

3.3 Dual Gate TFET Structure:

The intricate design of methane gas sensors requires a comprehensive understanding of the nuanced architecture of dual gate Tunnel Field-Effect Transistor (TFET) structures. Dual gate TFETs provide an elevated level of sensitivity, a critical factor for discerning minute variations in methane concentrations, aligning seamlessly with the project's objective of precision in gas detection. Leveraging the inherent low power consumption of dual gate TFETs enables the creation of energy-efficient sensors, a fundamental requirement for prolonged and eco-friendly operational use. This characteristic holds particular significance in applications like CNG vehicles and gas stations.

The efficiency of dual gate TFETs at low working voltages not only optimizes power consumption but also addresses the project's emphasis on energy efficiency in methane gas sensors. The high-speed operation of dual gate TFETs contributes to swift response times, enhancing the sensor's ability for real-time methane gas detection. The reduced heat generation in dual gate TFETs underscores the project's commitment to longevity and reliability, essential in scenarios demanding consistent and enduring sensor performance.

Exploring the material flexibility intrinsic to dual gate TFETs offers opportunities for optimizing material choices, tailoring the sensor design to specific environmental conditions. The compatibility of dual gate TFETs with cutting-edge technologies further solidifies the sensor's relevance in the dynamic field of gas detection and electronic components. Lastly, the integration and miniaturization capabilities of dual gate TFETs position them as fitting for

compact systems, addressing practical needs in applications like gas stations and CNG vehicles. Understanding the unique qualities of dual gate TFETs is pivotal for crafting sophisticated, energy-efficient, and sensitive methane gas sensors tailored for diverse real-world situations.

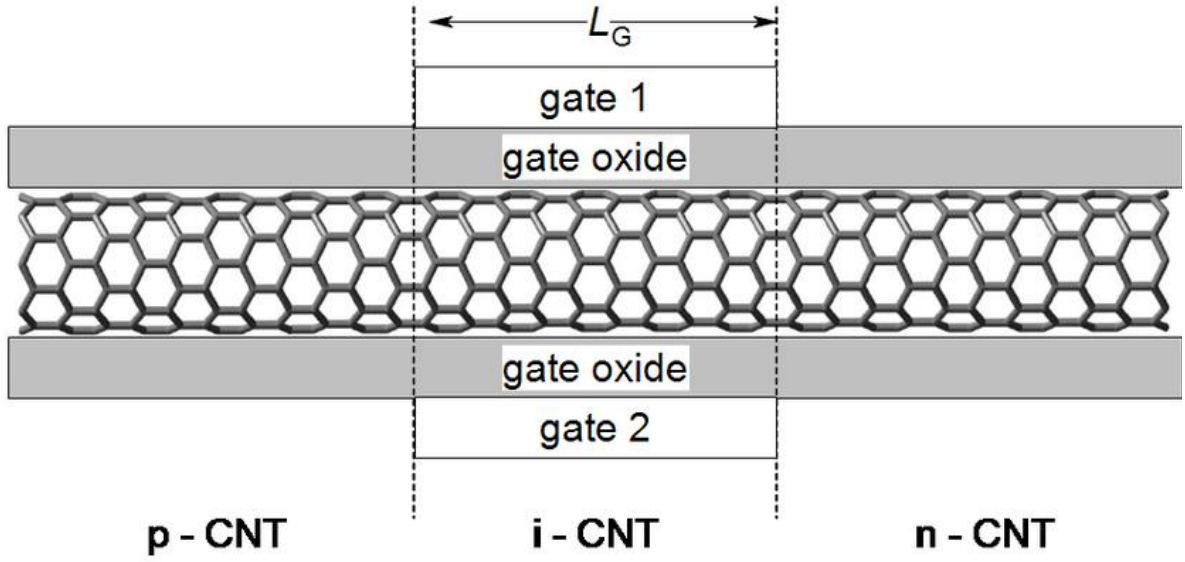

Figure 3.2: A dual gate TFET Structure

3.4 Dual-Gate TFET with BOX:

The ability of a Dual-Gate Tunnel Field-Effect Transistor (TFET) to considerably reduce leakage current and boost sensitivity when combined with Buried Oxide (BOX) is the driving force behind its inclusion in sensor design. The transistor's channel can be precisely controlled thanks to the dual-gate construction, which maximizes sensitivity for spotting minute variations in outside stimuli like gas concentrations. This increased sensitivity is especially useful for sensor applications where accuracy is crucial. At the same time, the channel's buried oxide layer reduces leakage current by reducing the amount of direct tunnelling current between the gates. The sensor's overall efficiency is improved by this decrease in leakage current, which makes it a good fit for applications where low-power operation is crucial.

Furthermore, the issue of short-channel effects, which are frequently present in smaller designs, is addressed by the dual-gate TFET with BOX. Even in tiny sensor setups, the buried oxide layer serves as a barrier to prevent short-channel effects and guarantee consistent transistor

functioning. Furthermore, the buried oxide layer's insulating qualities and the dual-gate structure's superior electrostatic control lead to an enhanced signal-to-noise ratio. This is vital for sensor applications where precise signal identification in a wide range of environmental circumstances is required. All things considered, dual-gate TFETs are promising options for creating highly effective, responsive, and adaptive sensors for a variety of real-world applications due to their compatibility with BOX with cutting-edge technologies and their versatility in material selection.

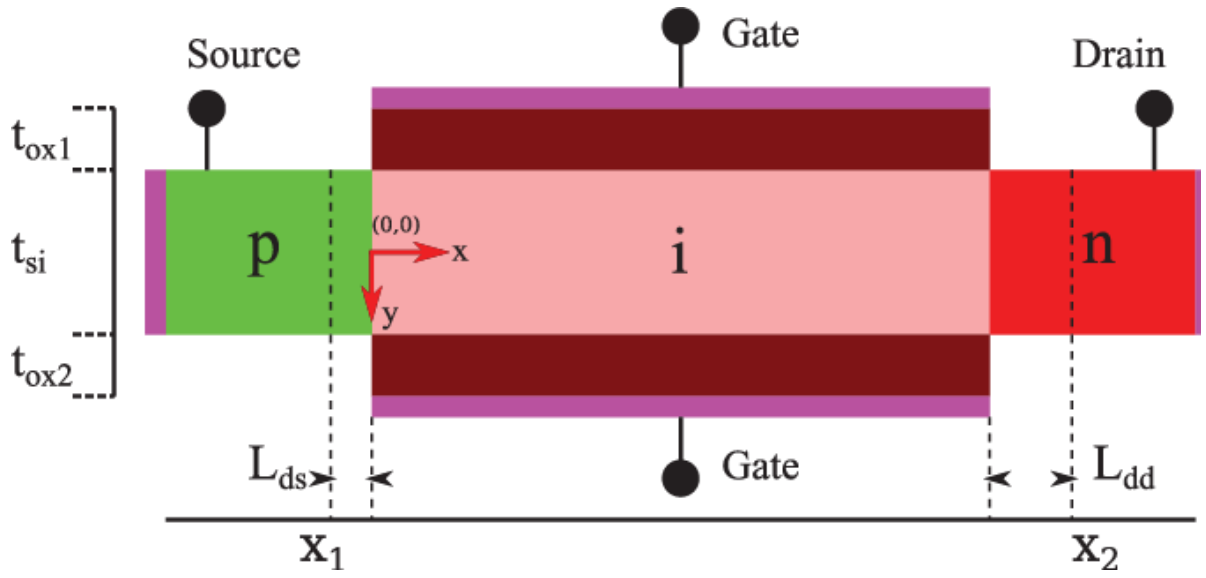

Figure 3.3: Dual-Gate TFET with BOX

3.5 Junctionless TFET for Sensor Design

In our project, we utilized a Junctionless Tunnel Field-Effect Transistor (TFET) to design the methane gas sensor. The junctionless TFET is characterized by uniformly doped source, drain, and channel regions, typically n-type, which eliminates abrupt junctions and simplifies fabrication.

- Source, Drain, and Channel: These regions are uniformly doped, removing the need for abrupt p-n junctions.

- Gate Electrode: Controls the current flow through the channel. By adjusting the gate voltage, the electric field in the channel can be modulated, influencing the tunnelling current.

- Biorecognition Elements: The channel surface is functionalized with elements that bind specifically to target biomolecules, crucial for detecting methane gas.

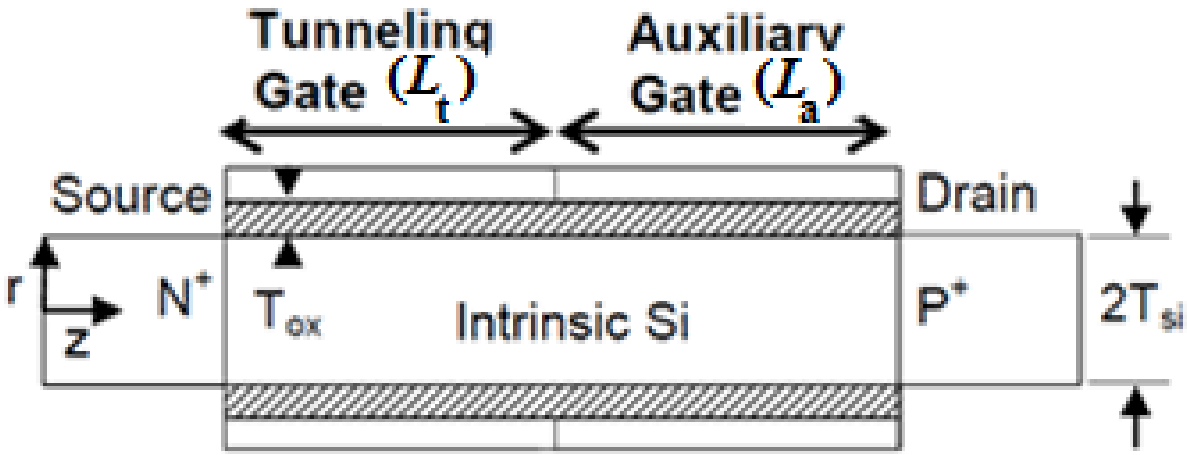

Figure 3.4: Junctionless TFET

3.5.1 Working Mechanism

- Biomolecule Binding and Surface Charge: When biomolecules, which carry inherent charges, bind to the biorecognition elements, they introduce additional charges at the interface between the channel and the gate dielectric, altering the surface potential.

- Energy Bands and Barrier Width: The change in surface potential affects the energy band structure, causing sharper bending of the energy bands and reducing the effective barrier width for tunnelling. This increased band bending facilitates easier tunnelling, enhancing the sensor's sensitivity and response.

Using a junctionless TFET for our sensor design offers advantages in simplicity, sensitivity, and reliability, making it an effective solution for detecting methane gas.

3.6 Software Tool Used

This project relies on simulation methods, with SILVACO ATLAS TCAD Tool serving as the primary software tool. Technology Computer-Aided Design (TCAD) involves using computer simulations to develop and refine semiconductor process technologies and devices. TCAD is a subset of electronic design automation, encompassing both Process TCAD, which

models semiconductor fabrication, and Device TCAD, which models device operation. Utilizing this tool offers the advantage of reducing development costs and shortening development timelines.

ATLAS Tool conducts physics-based simulations of semiconductor devices based on specified physical structures and bias conditions. It includes material properties for commonly used semiconductor materials. DeckBuild serves as the SILVACO editor, as depicted in Figure 3.1, facilitating the writing and simulation of codes. The code files are categorized into three types: ".in file" serves as the main editable file, ".str file" contains structure information, and ".log file" comprises all electrical data and calculated parameters post-simulation.

Tonyplot is employed as a graphical post-processing tool compatible with all SILVACo. simulators. It presents results from structure and log files in a visual format.

3.7 Device Specification

A junctionless tunnel field-effect transistor (TFET) designed for sensing applications typically features specific design parameters to enhance its sensitivity and performance. Here are the key device specifications and characteristics we consider:

3.7.1 Conventional Device Specifications

Device Structure

1. Channel Material: Typically, Silicon (Si) is used but alternative materials like germanium (Ge) or III-V compounds (e.g., InGaAs) can be employed for better performance.
2. Channel Length: Generally, ranges from 10 nm to 100 nm, with shorter channels offering higher sensitivity.
3. Channel Thickness: Around 5 nm to 20 nm, ensuring good gate control over the channel.
4. Gate Material: High-k dielectrics such as HfO2, with a typical thickness of 1 nm to 5 nm.
5. Gate Length: Usually matches the channel length, around 10 nm to 100 nm.
6. Gate Configuration: Can be single-gate, double-gate, or gate-all-around (GAA) for enhanced electrostatic control.

Electrical Characteristics

1. Threshold Voltage (v_{Th}): Tuned to be very low, often near or below 0.1V, to enable operation at low power.
2. Subthreshold Swing (SS): Ideally less than 60 mV/decade, much lower than conventional MOSFETs.
3. On-State Current (I_{ON}): Typically, in the range of µA/µm, depending on the application.
4. Off-State Current (I_{OFF}): Should be in the pA/µm range to minimize leakage.
5. Drain Voltage (v_D): Usually operates at low voltages, around 0.5V to 1V.

Performance Metrics

1. Sensitivity: High sensitivity to changes in the environment (e.g., gas molecules, biomolecules) due to the steep subthreshold slope and high surface-to-volume ratio.
2. Response Time: Fast response time, often in milliseconds, depending on the sensing mechanism.
3. Selectivity: Can be enhanced by functionalizing the gate or channel with specific receptors or using nanostructured materials.

Fabrication Considerations

1. Doping Concentration: Uniform doping throughout the channel, typically in the range of
N = 10^{17} cm^{-3} to 10^{18} cm^{-3}
2. Surface Passivation: To reduce surface states and improve stability.
3. Integration: Capable of being integrated with CMOS technology for on-chip applications.

These specifications provide a general guideline, but the exact parameters can be adjusted based on the specific sensing requirements and the materials and technologies available.

3.7.2 Proposed Device Structure

Specific Application

Gas Sensing: Functionalized with materials like metal oxides that will react with methane

Specification for a Junctionless TFET Sensor meant for sensing methane

- Channel Material: Silicon(Si)
- Channel Length: 100 nm
- Channel Thickness: 10 nm
- Gate1 Dielectric: Methane, 3 nm thick
- Gate2 Dielectric: PolySilicon, 3 nm thick
- Gate Length: 25 nm
- Drain Voltage: 0.5V-2.5V
- Functionalization: Specific to the target application (e.g., metal oxide for gas sensing, bioreceptors for biosensing)

3.8 How does the sensor work?

In this project, we are utilizing a junctionless Tunnel Field-Effect Transistor with a Boron Nitride (BN) sensing layer to detect methane gas. The choice of BN is due to its unique properties, such as high surface area, chemical stability, and the ability to interact effectively with gas molecules. The mechanism by which our sensor operates involves changes in the surface potential and subsequent modulation of the tunnelling current in the junctionless TFET structure.

3.8.1 Biomolecule Binding and Surface Charge

Methane molecules, when exposed to the BN sensing layer, interact with the surface, leading to the adsorption of methane on the BN surface. This interaction introduces additional charges at the interface between the BN layer and the channel of the junctionless TFET. The methane molecules, although non-polar, induce changes in the local charge distribution by altering the electronic environment of the BN surface. The adsorption process can be described by the Langmuir adsorption isotherm, given by:

$$\Theta = \frac{KP}{1+KP}$$

where Θ is the fractional coverage of the surface, K is the adsorption equilibrium constant, and P is the partial pressure of methane. This charge alteration is crucial as it modifies the electrostatic conditions at the surface of the channel, effectively changing the surface potential.

3.8.2 Modification of Surface Potential

The adsorption of methane on the BN layer leads to a change in the surface charge density, which in turn modifies the surface potential (ψ_s) of the channel. The surface potential represents the potential difference between the channel surface and the bulk of the semiconductor. The relationship between the surface charge density (σ) and the surface potential is given by:

$$\psi_s = \frac{\sigma}{\epsilon_s}$$

where ϵ_S is the permittivity of the semiconductor material. As methane molecules bind to the BN surface, they introduce additional charges or influence existing charge carriers, thereby altering (σ). This modification in surface potential impacts the energy band structure of the channel.

3.8.3 Impact on Energy Bands

The change in surface potential due to methane adsorption causes a shift in the energy bands at the semiconductor surface. This shift leads to more pronounced band bending near the surface of the channel. The relationship between the surface potential and the energy band bending can be described using Poisson's equation:

$$\frac{d^2\psi}{dx^2} = -\frac{\rho}{\epsilon_s}$$

where (ρ) is the charge density. In a junctionless TFET, where the source, drain, and channel are uniformly doped, this band bending is uniformly distributed. The increased band bending lowers the effective barrier for carrier tunnelling, facilitating easier tunnelling of charge carriers from the source to the drain through the channel.

3.8.4 Reduction of Effective Barrier Width

The sharper energy band bending resulting from the increased surface potential reduces the effective barrier width for quantum mechanical tunnelling. The tunnelling probability (T) is exponentially dependent on the barrier width (W) and can be described by the Wentzel-Kramers-Brillouin (WKB) approximation:

$$T \propto e^{\left(-\frac{2w\sqrt{2m*q(\phi_b)}}{h}\right)}$$

where m* is the effective mass of the charge carriers, q is the electronic charge, ϕ_b is the barrier height, and h is the reduced Planck constant. As the surface potential changes, the effective barrier width W decreases, increasing the tunnelling probability.

3.8.5 Increased Tunnelling Current

The reduction in the effective barrier width due to methane adsorption significantly increases the tunnelling current (I_D). The drain current in a TFET can be expressed as:

$$I_D \, \alpha \, T \propto (v_{DS} - v_{Th})$$

where (v_{DS}) is the drain-source voltage and (v_{Th}) is the threshold voltage. As methane molecules interact with the BN layer, the continuous change in surface potential dynamically adjusts the tunnelling barrier, thus modulating the tunnelling current. The relationship between the change in surface potential ($\Delta\psi_s$) and the change in drain current (ΔI_D) can be described by:

$$\Delta I_D \propto e^{\left(-\frac{2w\sqrt{2m*q(\phi_b-\Delta\psi_s)}}{h}\right)}$$

The increase in (ΔI_D) is directly proportional to the concentration of methane gas, making the junctionless FET with BN sensing layer highly sensitive to methane. This increased current serves as the primary signal for methane detection, where the magnitude of the current change correlates with the concentration of methane present.

3.8.6 Sensitivity and Response

The sensitivity (S) of the junctionless FET sensor can be quantified as:

$$S = \frac{\Delta I_D}{I_D} \times \frac{1}{\Delta C}$$

where (Δc) is the change in methane concentration. This equation highlights the proportional relationship between the drain current change and the concentration of methane, demonstrating the effectiveness of the sensor in detecting varying levels of methane gas.

3.9 Conclusion

In summary, our junctionless TFET with a Boron Nitride sensing layer detects methane gas by leveraging the interaction between methane molecules and the BN surface to alter the surface potential. This change in surface potential modulates the energy band bending and reduces the effective tunnelling barrier width, resulting in an increased tunnelling current. The sensor's operation is highly sensitive to the presence of methane, making it an effective tool for methane gas detection in various applications. This detailed explanation provides a comprehensive understanding of the working mechanism of our Boron Nitride-based junctionless FET methane sensor, highlighting the critical steps and the physical principles underlying its operation. The theoretical considerations, fabrication process, and practical implementation discussed here ensure that our sensor design is robust, efficient, and capable of meeting real-world detection requirements.

CHAPTER 4

IMPLEMENTATION OF A DUAL SOURCE SOI TFET FOR INVERTER APPLICATION

4.1 Introduction

Miniaturization of device sizes has allowed to accomplish the objective of low-power, high-speed devices with increased package density, which enhances the RF performance throughout the last few decades. However, MOSFETs suffer from short channel effects such as DIBL, threshold voltage roll-off, high leakage, and others due to rigorous scaling of channel length. MOSFET SS is also restricted to 60mV/dec. Due to band-to-band tunnelling processes, TFET can overcome MOSFET's drawbacks. TFET also has a steeper SS. In addition, the SS in TFET is steeper. As a result, the TFET is becoming a promising low-power technology thanks to supply voltage scaling. However, because to the BTBT limitation, TFET has a lower ION than MOSFET. As a result, the switching delay (CV_{DD}/I_{ON}) increases. Several structural changes have been carefully investigated to solve this problem [29-38]. To obtain superior SS and greater I_{ON}/I_{OFF}, U-shape [39], L-shape [40], and TRS-shape [41] TFETs have recently been used to enhance tunnelling area. Quantum confinement effects (QCE) affect TFETs with features smaller than or equal to 20nm. Yu and Najam investigated the influence of geometrical QCE on the performance of L-TFET in 2019 [42-43].

Following the semiconductor industry's plan, a new barrier emerges in the form of a small tunnelling area in TFET, which results in a small tunnelling current. Due to the concentrated and confined tunnelling region in TFET, it has been observed that the tunnelling current is constant with respect to the channel length [44],[45]. During the circuit design phase, this event allows for modifying the device driving capabilities to meet the practical demands. The Double Source TFET is proposed to overcome this drawback. In addition, the proposed highly scalable symmetrical DSS n and p-type TFETs use a quantum simulation-based method to enhance device ON current and reduce ambipolarity while retaining almost uniform SS at varied gate lengths. Before going for any digital or analog circuit level application, the very first step is to design an inverter. However, both the n-TFET and the p-TFET should be designed appropriately to comply with the CMOS characteristics by suppressing the ambipolar current for complementary performance [46]. The manuscript is organized in the following manner In Section II, the device structure has been discussed along with simulation Setup, fabrication process and the calibration of the device models. In section III,the simulated resulted related to

the proposed device has been studied. The circuit-level analysis has been performed in section IV and at last the manuscript is concluded in section V.

4.2 Device Specification

Figs 4.1(a) and 4.11(b) show the 2D cross sectional view of the proposed n and p-type DSS TFETs (b). Although the size of both TFETs are identical, the doping options have been chosen based on the kind of TFET. Source1 and Source2 are two distinct highly doped Sources in the proposed structures. Both TFETs have a narrow lightly doped region next to the source, as illustrated in Fig 4.1. At the source channel junction, this structural variation helps in the introduction of the inter band tunnelling phenomenon. Because the two sources have distinct structural positions, both TFETs can be considered to have two channels (right and left channel). A lightly doped Si layer (p-type for n-TFET or vice versa) has been introduced below the abovementioned two channels to enhance carrier transport from the two sources to drain. As a result, in both situations, it behaves as a horizontal channel. A SiO_2 box has been incorporated between the drain and source2 region to prevent drain leakage. Different effective channel lengths, such as 5nm, 7nm, 9nm, 13nm, and 20nm, have been used to investigate the performance of both TFETs. Fig 4.1 depicts the critical parameters for the two devices.

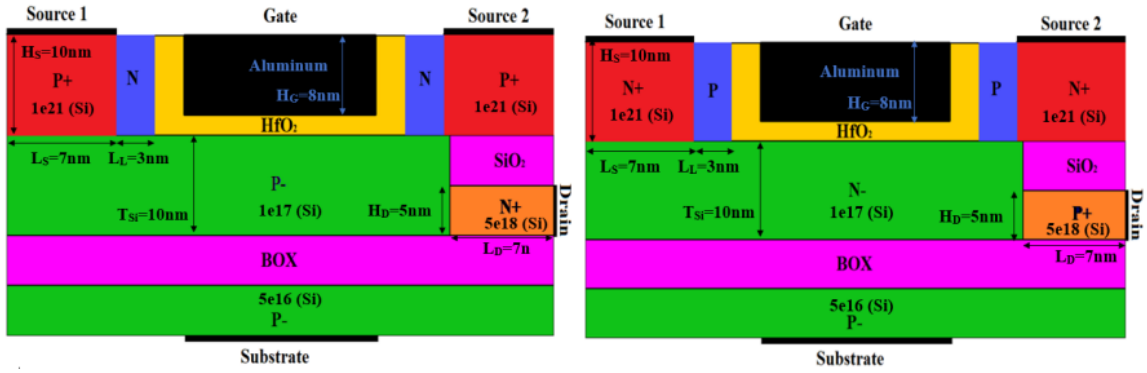

Fig 4.1. Device structure of (a) n and (b) p-type DSS-TFET

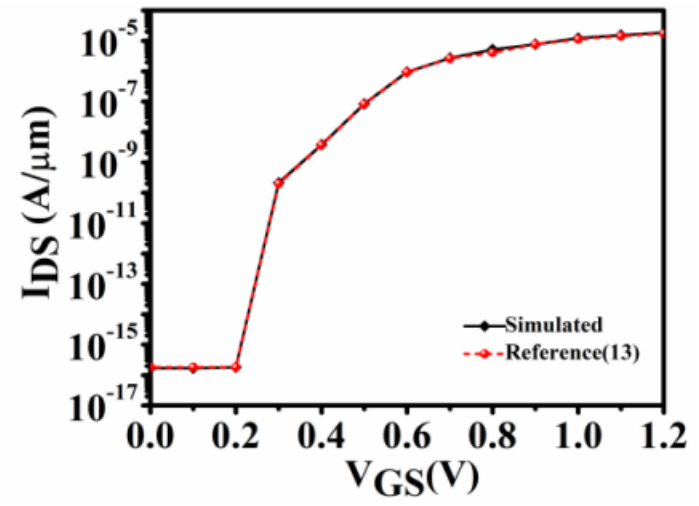

Fig 4.2: Calibration of simulation data with the experimental result of Reference [41].

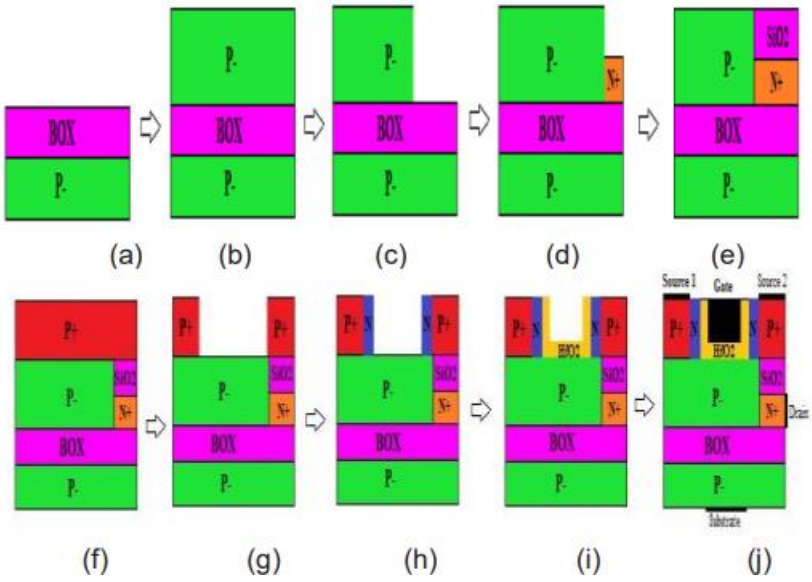

Fig 4.3: Process flow for the fabrication of the proposed DSS- TFET structure

For simulation SILVACO ATLAS has been incorporated. During simulation, many essential models such as CVT, band gap narrowing, non-local BTBT, drift diffusion carrier transport, SRH and Auger recombination and FD statistics were incorporated. The generating rate is calculated using the BTBT model. To account for ambipolar conduction, it will establish a quantum tunnelling region at both junctions. The FD statistics model was used to account for the influence of carrier concentration on device performance. The Auger and SRH recombination models have been used to account for the influence of carrier energy exchange with the surrounding lattice as well as the carrier's life period. The DSS-TFET simulated result

has also been calibrated with [41]. Fig.4.2 shows a reasonable agreement between the two outcomes, indicating that the chosen models are genuine.

Fig. 4.3 depicts the manufacturing procedures for the proposed DSS-TFET. As shown in Fig. 4.3, it starts with the creation of a thick buried oxide layer on a p-type silicon wafer using the traditional separation approach [41]. Following that, a lightly doped p-type silicon was produced followed by a highly doped n-type drain slab using epitaxy to construct the channel and drain, as shown in Fig. 4.3(b)- (d). Fig. 4.3(e) shows the oxidation process depositing SiO_2 across the drain area. To form the (a) (b) Fig4.1. Device structure of (a) n and (b) p-type DSS-TFET Fig 4.2. Calibration of simulation data with the experimental result of Reference [13]. (a) (b) (c) (d) (e) (f) (g) (h) (i) (j) Fig 4.3. Process flow for the fabrication of the proposed DSS-TFET structure double source, a highly doped P-type is grown using epitaxy process as per Fig. 4.3 (f). To evolve the sources, a U-shaped window is etched out from the highly doped silicon substrate as shown in Fig. 4.3 (g), followed by epitaxy process two pockets of n-type besides the both sources grown to enhance the tunnelling shown in Fig. 4.3(h). Then, as illustrated in Fig. 4.3(i), high-k gate oxide was deposited over the U-shaped trench area using the Atomic Layer Deposition (ALD) method. Finally, as illustrated in Fig. 4.3 (j), the gate is deposited and patterned before the contacts are defined at their corresponding locations.

4.3 Results and Discussion

4.3.1 Transfer Characteristics of proposed TFETs for Various Channel length

At V_{DS}=0.1V, Fig. 4 shows the I–V characteristics of both p-type and n-type DSS-TFETs. Both structures outperform [5], [8], and [11] in terms of I_{ON}/I_{OFF}. It's worth noting that when the channel length is less than 20nm, the on and off current for both TFETs is nearly constant. As a result, the suggested device can be inferred to be scalable throughout a range of channel lengths from 5nm to 13nm.

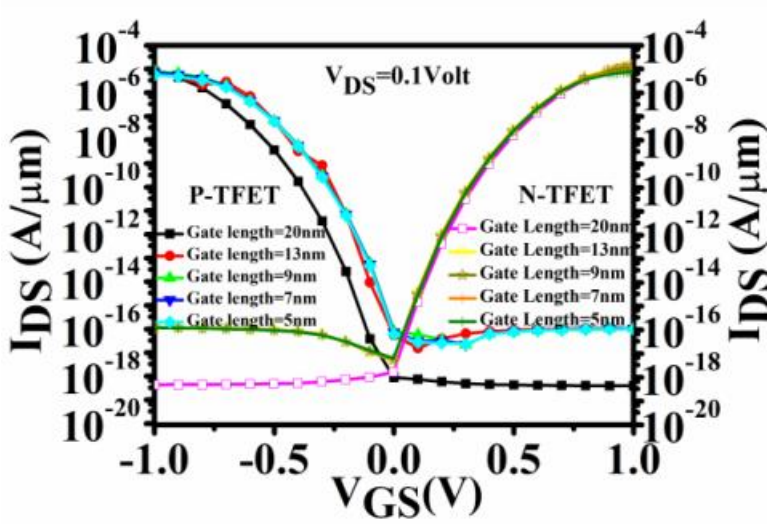

Fig 4.4: I–V characteristics for both n and p- type DSS-TFET at V_{DS}=0.1V

The structure is robust and scalable even at the quantum level, as shown in Fig. 4.5. There is negligible change in SS for both TFETs at varied gate lengths, as shown in Fig.4. 5.

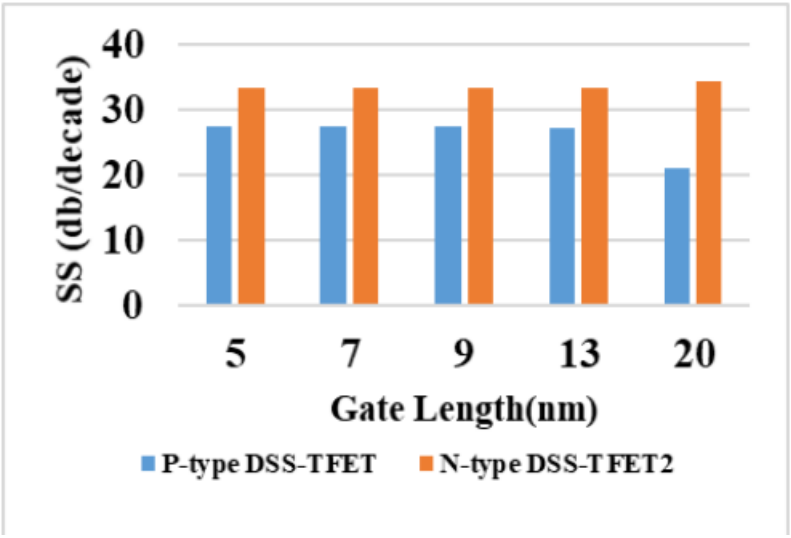

Fig 4.5: Comparison of Subthreshold Swing for both n-type and p-type SDS-TFET at V_{DS}=0.1V

4.3.2 Variation of Oxide Thickness

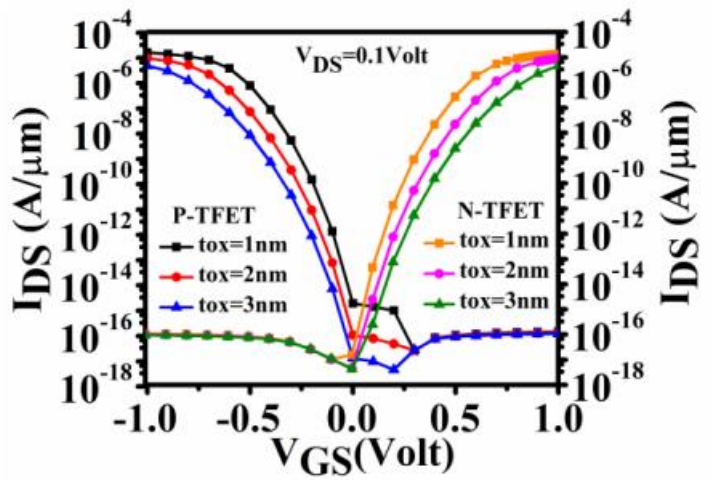

Fig 4.6: Variation of oxide thickness for both n-type and p- type DSS-TFET at V_{DS}=0.1V

For several uniform gate oxide thicknesses such as 3nm, 2nm, and 1nm, the transfer characteristics of the proposed DSSTFETs have been investigated. Fig 4.6 demonstrates that the performance of both TFETs with a 1nm gate oxide thickness outperforms the other two. However, as stated in [39], there is a chance that I_{ON}/I_{OFF} will degrade as ambipolarity increases. As a result, the suggested structural device is based on a 2nm gate oxide thickness.

4.3.3 Variation of Gate Work Function

In both n-type and p-type DSS-TFETs, the effect of gate work function variation is seen in Fig 5. Drain-channel tunnelling reduces when gate work function lowers, but source-channel tunnelling rises, as seen in traditional TFETs [39]. According to [18], in order to offer comprehensive CMOS logic functionality, ambipolar current suppression in TFETs is required for circuit design. Fig 5 shows that the proposed DSS-TFET, which has a 13nm gate length and a 2-nm oxide thickness, as well as a work function of 4.95 for n-type and 4.45 for p-type, suppresses the ambipolar current and is thus suitable for TFET inverter design.

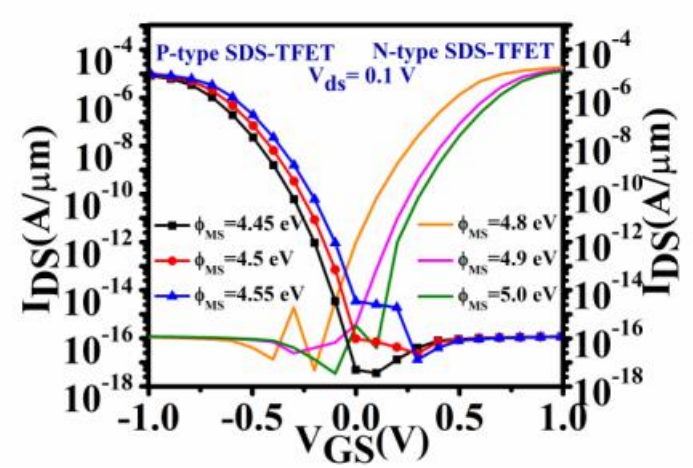

Fig 4.7: Variation of Gate Work function for both n and p-type DSS-TFET at V_{DS}=0.1V

4.3.4 Total Current Density & Band to Band Tunnelling (BTBT)

Figs 4.8 and 4.9 show contour plots of total current densities for both DSS-TFETs. The tunnelling may be seen coming from both the source and channel junctions. Tunnelling is more common between source-2 and channel junction than between source-1 and channel junction.

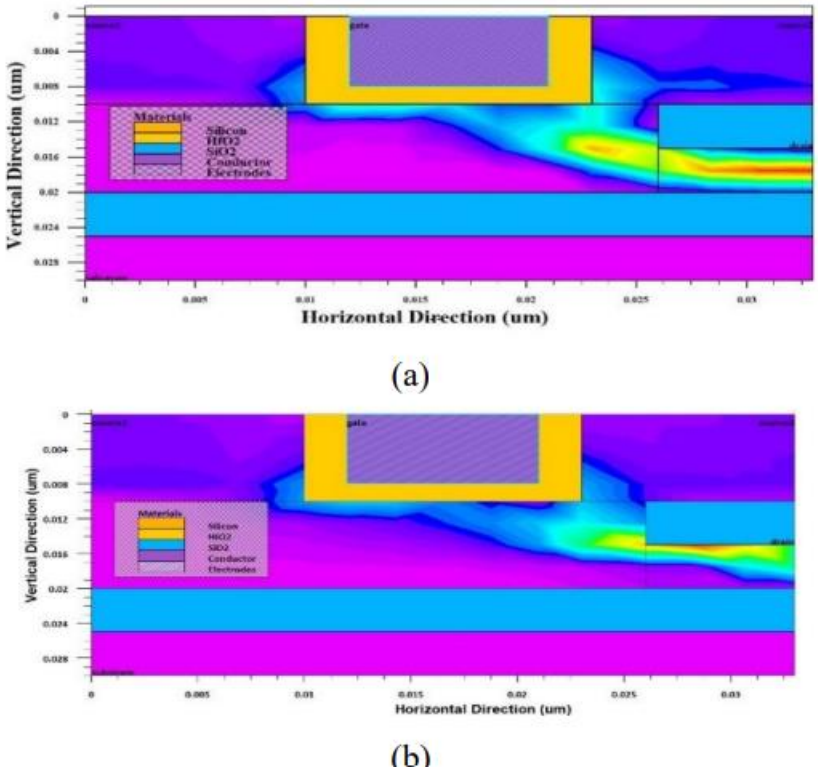

Fig 4.8: Total Current Density of 13-nm gate length (a) n-type and (b) p-type DSS-TFET

This is due to the fact that the drain is located directly under the source- 2. So, for this DSS-TFET, source 2 can be regarded the main source. Source-1 is acting as a buried source, providing additional bust to enhance I_{ON} and therefore give device structural stability, as evidenced by the low fluctuation in slope of the transfer characteristics displayed in Fig4. 2. Fig 4.7. depict BTBT for both the DSS-TFETs at a 13-nm gate length, where source-2 functions as the principal source and source-1 acts as a buried source to offer added bust to tunnelling processes.

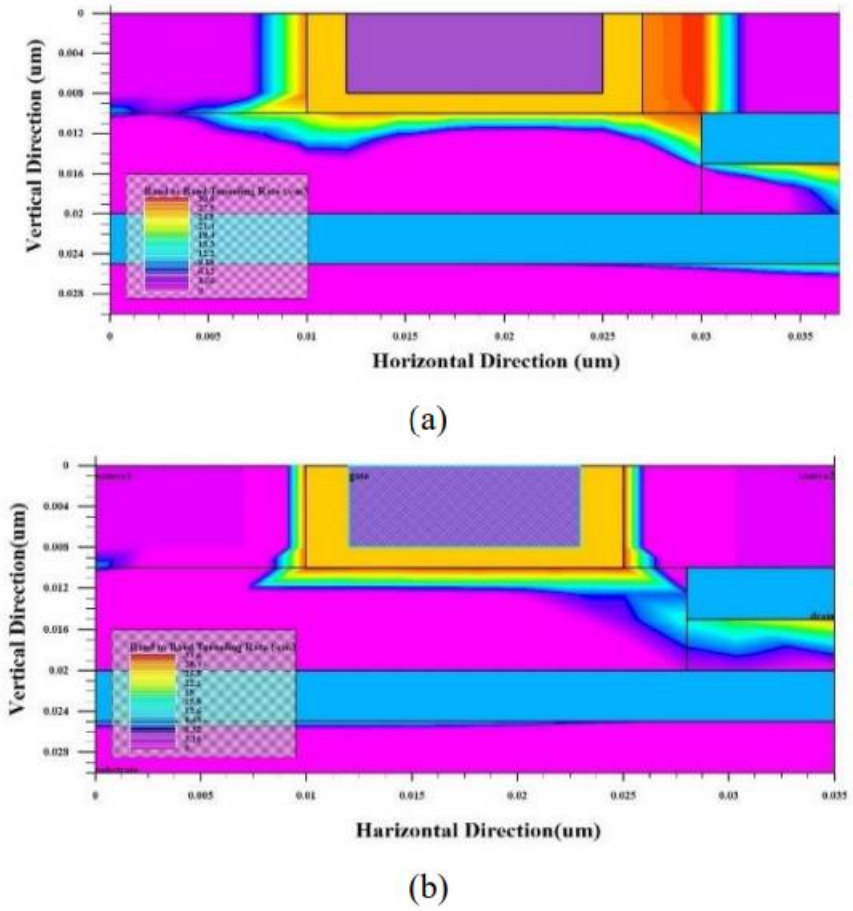

Fig 4.9: BTBT rate of 13-nm gate length (a) n-type and (b) p-type DSS-TFET

4.3.5 Output Characteristic of proposed DSS-TFETs

Fig 10 shows the output characteristics of p-type and n-type DSS-TFETs at various VGS. When compared to the current of a p-type DSS-TFET at the same V_{GS}, the n-type DSS-TFET has approximately three times the amplification. As a result, the width of the source of p-type DSS-TFET must be expanded by three times [12] in order to obtain the same amplification for an appropriate inverter design.

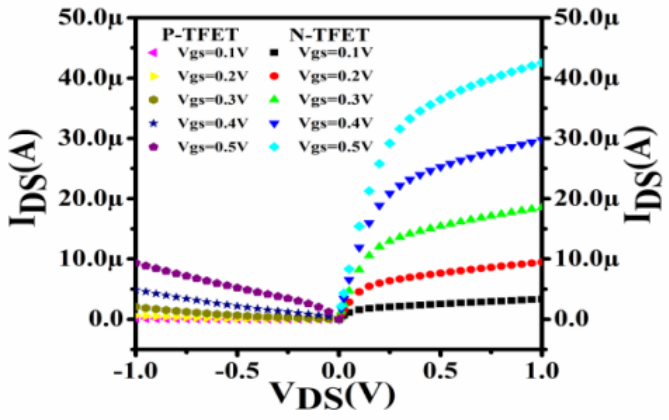

Fig 4.10: I_{DS}-V_{DS} curve for both p-type and n-type DSS-TFET at different V_{GS}

4.3.6 Comparison of Cut-off Frequency and Transconductance of DSS-TFET

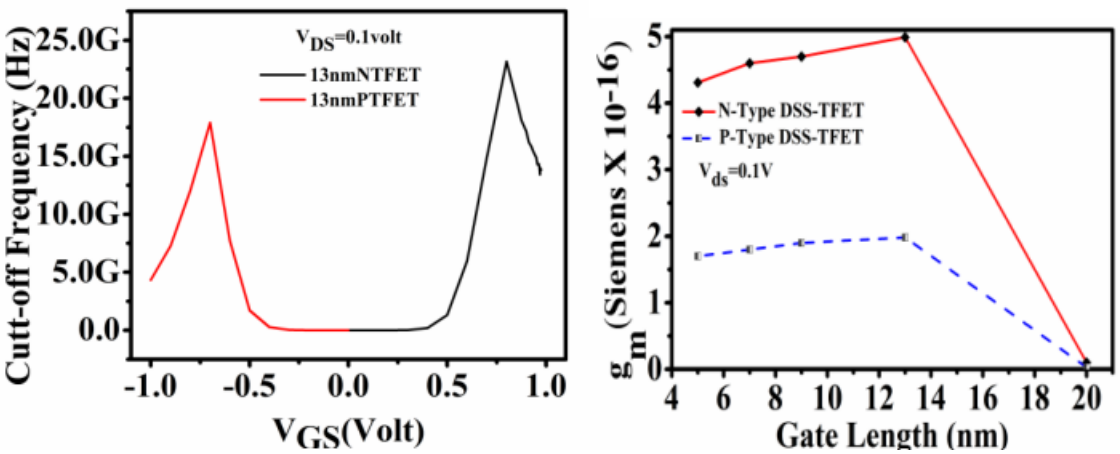

Fig 4.11: Comparative plot of Cut-off Frequency (f_T) with respect to V_{GS} of both n-type and p-type SDS-TFET at V_{DS}=0.1V

Fig. 4.12: Comparison of transconductance for both n-type and p-type SDS-TFET at V_{DS}=0.1V

The cut-off frequency (f_T) and GBP are critical factors to consider when analyzing the RF performance of any FET device. The cutoff frequency is defined as the frequency at which the short-circuited current gain equals one, as illustrated in Fig. 4.11, which shows a comparison of f_T plots for N-type and P-type SDS-TFETs. The f_T is given by,

$$f_T = \frac{g_m}{2\pi(C_{gd}+C_{gs})}$$

Where g_m is the transconductance. DSS-TFET has cut-off frequency f_T=24GHz for n-type TFET and f_T=17 GHz for p-type TFET, when gate length is 13nm. This can also be justified from the comparison plot of transconductance of the DSS-TFET shown in Fig.4.12, due to a larger gm for gate length 13 nm compare to others. This is due to the fact that f_T rises with the VGS at first due to the increase in gm, but beyond a certain V_{GS}, it starts to drop due to the decrease in g_m at a higher V_{GS} due to mobility degradation [34].

As a result, it's clear that the proposed DSS-TFET with a gate length of 13nm is more suited for dc and RF performance than existing TFET devices.

4.4 Circuit-Level Analysis

A basic digital inverter using the proposed n and p-type DSS-TFETs has been designed. In order to test the feasibility of the proposed devices in circuit applications, two sets of lookup tables of current and capacitances which includes I_{DS} (V_{GS}-V_{DS}), C_{GD} (V_{GS}- V_{DS}), C_{GS} (V_{GS}-V_{DS}) are constructed using the data exported from SILVACO TCAD. The lookup tables are then implemented in SPICE with the help of Verilog-A model. At first the inverter is investigated thoroughly with the help of these models. Then, logic gates such as NAND and NOR, have been designed and investigated in terms of power and delay at a particular supply voltage.

Fig. 4.13 depicts the inverter's schematic. Both transistors have a channel length of 13 nm. The n-TFET transistor has a width of 10 nm, whereas the p-TFET transistor has a width of 30 nm [35]. With a supply voltage ranging from 0.2 V to 0.5 V, the inverter circuit's DC performance is measured in terms of noise margin (NM). The noise margin is the difference between the input and output thresholds.

Vin	Vout
1	0
0	1
1	0

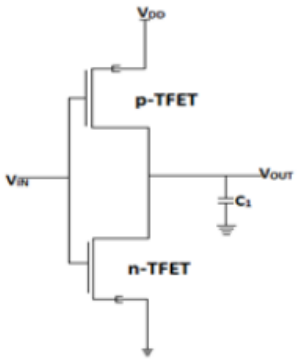

Fig 4.13. (a)Proposed Inverter consisting of DSS-TFET(b) Truth Table

According to Fig 4.14. (a), as V_{DD} decreases, the proposed inverter's VTC shape approaches that of a perfect CMOS inverter, and at V_{DD}=0.2V, it is nearly identical to a CMOS inverter. The simulated VTC indicates that the inverter's transition voltage is approximately $V_{DD}/2$ and that the high and low levels are clearly separated, indicating that both devices are operational. The suggested inverter's voltage gain (V_{OUT}/V_{IN}) is shown in Fig 4.14. (b). Because of the higher I_{ON} and improved ambipolarity, a voltage gain of 16 is nevertheless attained at V_{DD}=0.2V, indicating a great potential for low power applications

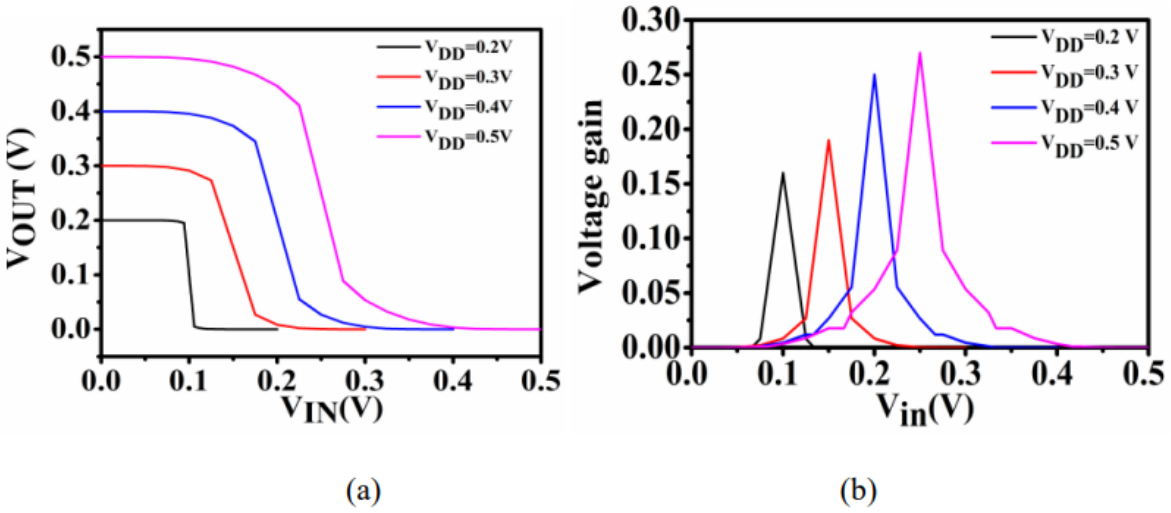

Fig 4.14. (a) VTC of the DSS-TFET inverter with V_{DD} varied from 0.2 V to 0.5 V (b) voltage gain of the DSS-TFET inverter under various V_{DD}, showing high gain even at V_{DD} = 0.2 V.

Fig. 4.15 illustrates the VTC of the proposed DSS-TFET inverter at V_{DD}=0.2V in order to evaluate the noise margin. The values VIL and VIH represent the input voltages for which the inverter's voltage gain dV_{OUT}/dV_{IN} =-1. The output voltages V_{OL} and V_{OH} may also be determined from the transfer characteristics by taking into account the minimum and maximum

voltage values. The formulae below can be used to determine the low noise margin (NML) and high noise margin (NMH),

$NM_H = V_{OH} - V_{IH}$

$NM_L = V_{IL} - V_{OL}$

Table 4.1. lists the DC parameters associated to VTC. The proposed inverter has a high to low noise margin around 97% at V_{DD}=0.2 volt, indicates that it almost behaves like an Ideal CMOS inverter.

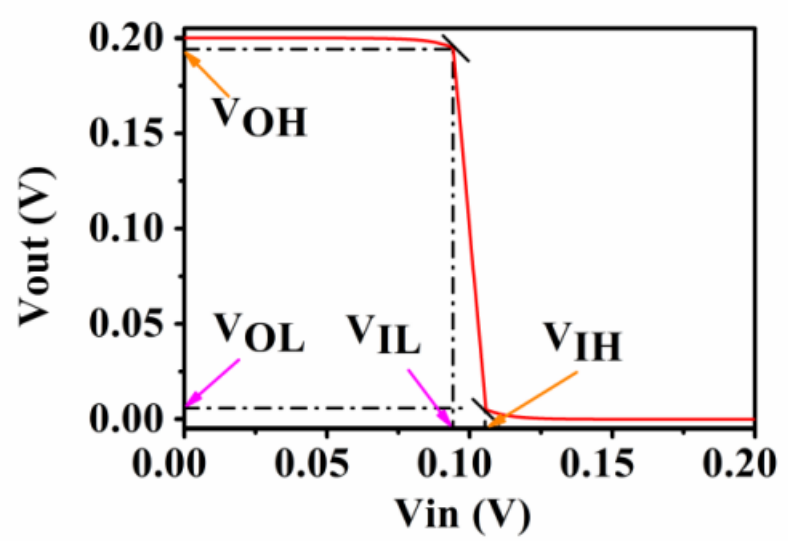

Fig 4.15. VTCs of the proposed inverter at V_{DD}=0.2 V

Parameters	DC Value
V_{IL}	9.43 mV
V_{OL}	4.99 mV
V_{IH}	105.75 mV
V_{OH}	194 mV
$N_{ML} = V_{IL} - V_{OL}$	89.32 mV
$N_{MH} = V_{OH} = V_{IH}$	88.35mV

Table 4.1. Different DC parameters of the inverter based on our proposed structure of TFET

4.5 Conclusion

The article proved that the TFET may be used as a low-power VLSI design alternative to today's CMOS technology. At a lower VDS=0.1volt, both n-type and p-type DSS-TFETs generate greater I_{ON}/I_{OFF} ratios of 10^{13} for n-type and 10^{12} for p-type respectively, with minimal ambipolar current. Because the difference in SS is almost negligible for different channel lengths, both TFETs are extremely scalable. As a result of, the 13nm n-type and 5nm p-type DSSTFETs may be incorporated during circuit design, resulting in a decrease in chip area. This is the primary benefit of the proposed device. From the VTC curve of the proposed inverter, it is evident that the high to low noise margin is of 97% which justifies the proposed inverter is almost identical to a CMOS inverter and a having a higher voltage gain of 16 at supply voltage of 0.2V. Also, from the power consumption, delay and PDP point of view, the proposed logic gates are superior than the compared TFET based logic gates [47-48].

In conclusion, our journey in exploring the potential of dual-source Silicon-On-Insulator (SOI) Tunnel Field Effect Transistor (TFET) has been both enlightening and transformative. Beginning with its application as a CMOS inverter, we delved deeper into its capabilities as a sensor, specifically for methane detection. While the dual-source SOI TFET showed promise, the realities of fabrication difficulties and high costs led us to consider alternatives. Recognizing the pragmatic concerns in our context, we transitioned to a junctionless TFET, a more cost-effective solution that resonates with the needs of our community.

Our focus on the single-layer dual-gate junctionless TFET proved to be a strategic decision, showcasing remarkable efficacy in detecting methane gas leaks. We had also considered the multiple layer option for the junctionless TFET, but went ahead with the single layered one due to its unique advantages. While acknowledging the potential of the former model, our choice reflects a balance between functionality, feasibility, and accessibility. Navigating this in the next chapter, we have not only identified a viable sensing solution but also underscored the importance of aligning technological innovation with real-world constraints and demands.

CHAPTER 5

DESIGN AND ANALYSIS OF A JUNCTIONLESS FET FOR SENSING APPLICATIONS

5.1 Introduction

The analysis of the high-sensitivity methane sensor's performance, leveraging Junctionless Field-Effect Transistors (JLFETs), is conducted through a series of comparative and overlaid graphs, each focusing on critical parameters.

Initially, doping concentration-based voltage-current characteristics are examined to determine the optimal doping level. This step is essential for identifying the doping concentration that maximizes sensitivity and minimizes interference.

Subsequently, voltage-current graphs are plotted against varying V_{DD} (drain-to-source voltage) at the identified ideal doping concentration. This exploration aims to establish the most efficient operational voltage for the sensor.

Following the determination of the optimal V_{DD}, the impact of temperature variations on the voltage-current characteristics is investigated. This analysis ensures the sensor's reliability and stability under different environmental conditions, presenting voltage-current graphs against changing temperature in Kelvin.

Finally, at the ideal temperature, detailed individual graphs are presented. These include voltage-current characteristics, band-to-band tunnelling rate, conduction band versus valence band interactions, electric field distribution, and potential. These graphs provide a comprehensive view of the sensor’s performance and the underlying physical phenomena.

The comprehensive nature of this analysis ensures that each critical parameter is thoroughly evaluated, enabling a robust understanding of the sensor’s capabilities and limitations. By methodically varying doping concentrations, operational voltages, and temperatures, the study addresses the multifaceted challenges of methane detection in CNG environments.

In summary, the detailed investigation into the JLFET-based methane sensor underscores its potential to significantly enhance safety in CNG applications. The findings not only demonstrate the sensor’s high sensitivity and reliability but also contribute to the broader goal of developing sustainable and safe energy solutions. This research paves the way for further

advancements in methane detection technology, promoting the continued viability of CNG as a clean energy alternative.

5.2 VI-characteristics against different doping concentrations

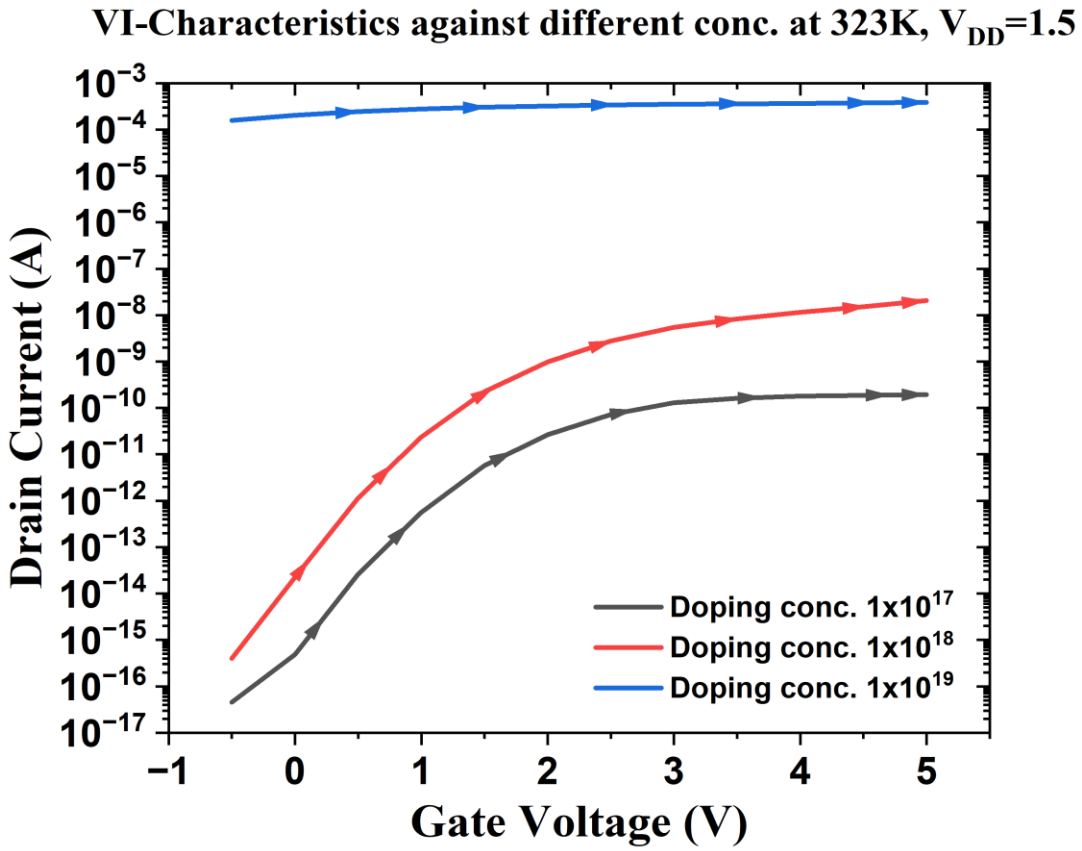

Fig 5.1: VI-Characteristic overlay graphs against different doping concentrations at 323K, $V_{DD=}$1.5V

Based on the curves, the doping concentration of 1×10^{18} atoms/cm^3 (green curve) appears to be the most suitable choice as it provides a good balance between ON-state current (high enough for reasonable drive current) and OFF-state current (low enough for adequate leakage suppression).

The lower doping concentration of 1×10^{17} atoms/cm^3 (red curve) results in a lower ON-state current, which may limit the device's performance, while the higher doping concentration of 1×10^{19} atoms/cm^3 (blue curve) exhibits a higher OFF-state current, indicating higher leakage and potentially higher power consumption.

Therefore, the decision to move forward with a doping concentration of 1×10^{18} atoms/cm^3 is a reasonable choice, as it optimizes the trade-off between drive current and leakage current for this particular TFET device.

5.*3 VI-characteristics at 323K against different drain voltages*

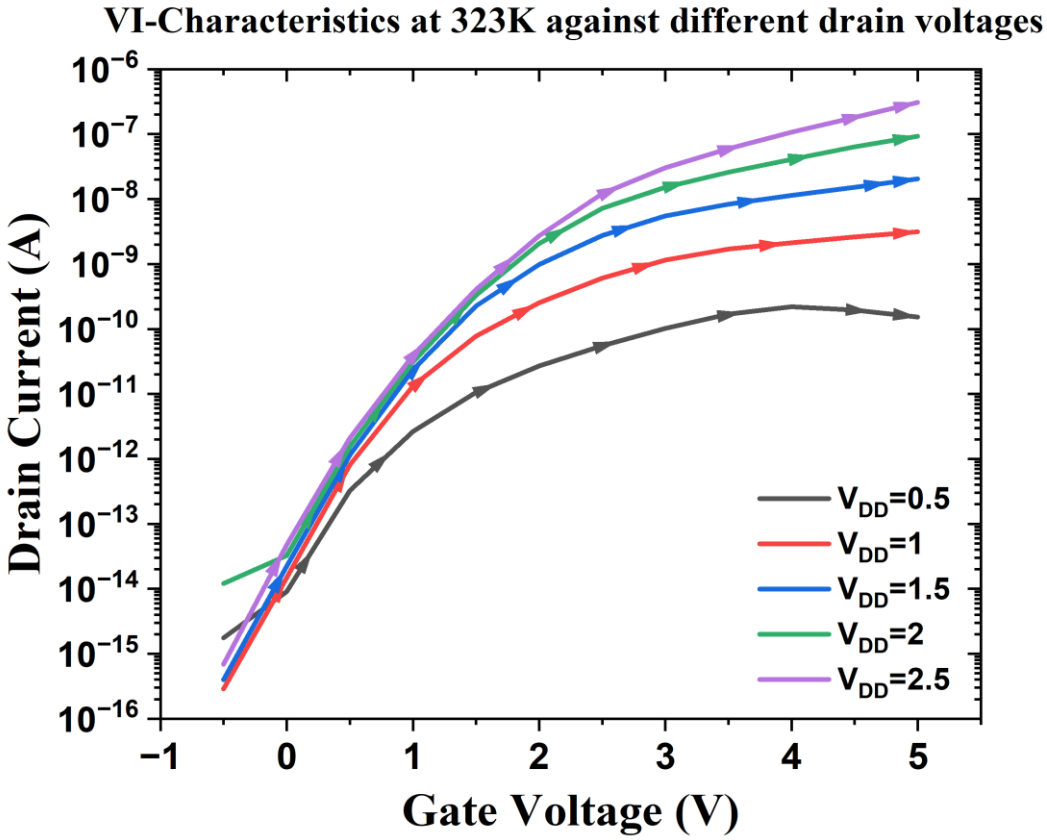

Fig 5.2: VI-Characteristics overlay graphs against different drain voltages (V_{DD})

This graph shows the transfer characteristic curves (drain current vs. gate voltage) for the junctionless TFET at a fixed doping concentration (1×10^{18} atoms/cm^3 based on the previous graph) and temperature (323K), but with varying drain voltages (V_{DD}) ranging from 0.5V to 2.5V.

Higher drain voltages generally lead to higher ON-state currents, as evident from the upward shift of the curves with increasing V_{DD}. However, higher V_{DD} also results in increased OFF-state leakage currents and power consumption.

The curve corresponding to V_{DD} = 1.5V (purple) appears to strike a reasonable balance between ON-state performance and OFF-state leakage. At this drain voltage, the ON-state current is

sufficiently high for acceptable drive strength, while the OFF-state current is relatively low, contributing to lower static power dissipation.

Moving forward with V_{DD} = 1.5V is a judicious choice, as it optimizes the trade-off between drive current and leakage current for this particular TFET device at the given doping concentration and temperature. This operating voltage should provide adequate performance while maintaining reasonable power efficiency.

5.4 VI-characteristics at V_{DD}=1.5 V against different temperatures

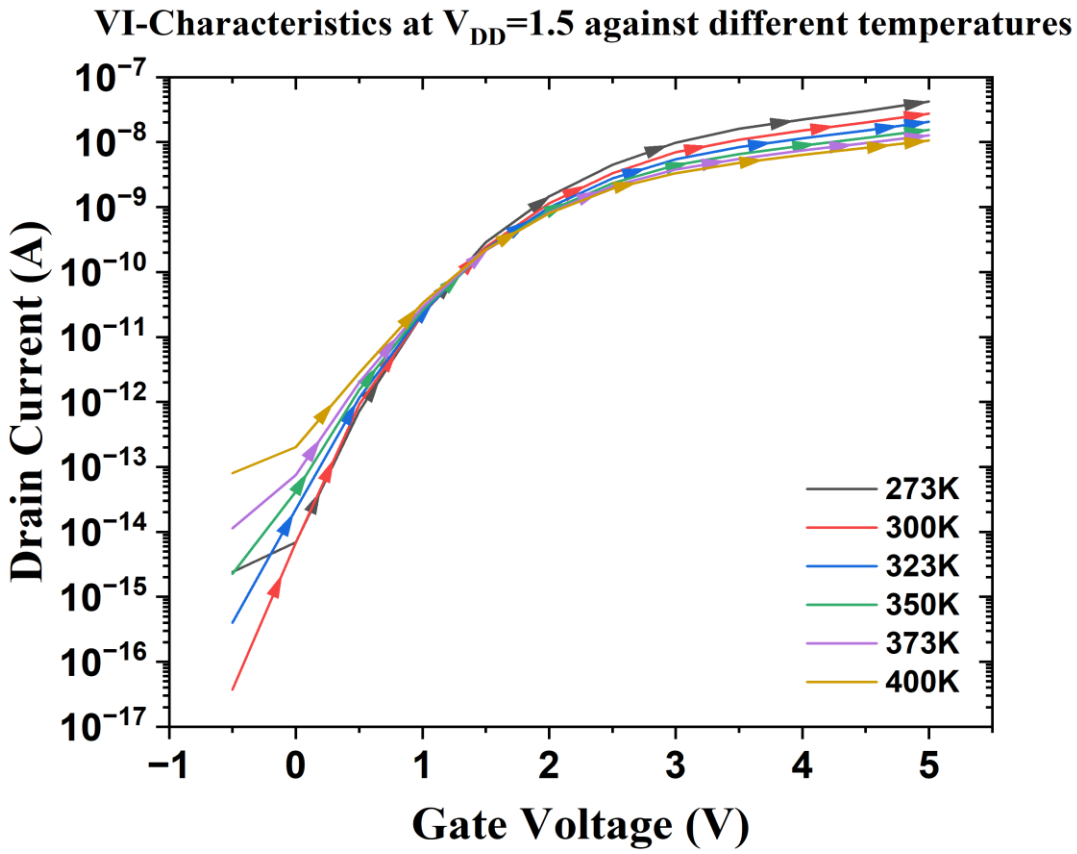

Fig 5.3: VI-Characteristic overlay graphs against different temperatures (in Kelvin)

This graph shows the transfer characteristic curves (drain current vs. gate voltage) for the junctionless TFET at the previously determined optimal doping concentration (1×10^{18} atoms/cm^3) and drain voltage (V = 1.5V), but with varying temperatures ranging from 273K to 400K.

The curves reveal that as the temperature increases, the overall drain current (both ON-state and OFF-state) increases. This is due to the increased thermal energy of charge carriers, which enhances their ability to overcome potential barriers and contribute to the current flow.

However, the increase in OFF-state current with temperature is undesirable as it leads to higher static power dissipation and can degrade the device's performance and energy efficiency.

The curve corresponding to 323K (green) appears to strike a good balance between ON-state performance and OFF-state leakage. At this temperature, the ON-state current is reasonably high, enabling sufficient drive strength, while the OFF-state current is relatively low, minimizing static power consumption.

Moving forward with a temperature of 323K is a judicious choice, as it optimizes the trade-off between drive current and leakage current for this particular TFET device at the given doping concentration and operating voltage. This temperature should provide adequate performance while maintaining reasonable power efficiency and minimizing detrimental temperature effects.

5.5 Tabular Analysis

Doping Concentration	Gate 1 Work Function	Gate 2 Work Function	Temperature	On-Off	Slope	V_{DD}	V_{GS}
10^{17}	12.65	3.9	323K	10^{6}	32	1.5 V	0.5 V – 5 V
10^{18}	12.65	3.9	323K	10^{8}	50	1 V	0.5 V – 5 V
10^{18}	12.65	3.9	273K	10^{8}	50	1.5 V	0.5 V – 5 V
10^{18}	12.65	3.9	323K	10^{6}	55	0.5 V	0.5 V – 5 V
*10^{18}	12.65	3.9	323K	10^{8}	55	1.5 V	0.5 V – 5 V
*10^{18}	12.65	3.9	323K	10^{8}	55	1.5 V	0.5 V – 5 V
10^{18}	12.65	3.9	300K	10^{10}	57	1.5 V	0.5 V – 5 V
10^{18}	12.65	3.9	323K	10^{7}	59	2 V	0.5 V – 5 V
10^{18}	12.65	3.9	350K	10^{7}	61	1.5 V	0.5 V – 5 V
10^{18}	12.65	3.9	373K	10^{6}	65	1.5 V	0.5 V – 5 V
10^{18}	12.65	3.9	323K	10^{8}	66	2.5 V	0.5 V – 5 V
10^{18}	12.65	3.9	400K	10^{5}	75	1.5 V	0.5 V – 5 V
10^{19}	12.65	3.9	323K	10^{1}	88	1.5 V	0.5 V – 5 V

Table 5.1: Tabular analysis based on different parameters for the proposed structure

Note: * denotes the ideal parameters for the Junctionless-TFET

In conclusion, the analysis of Junctionless Tunnel Field-Effect Transistors (JL-TFETs) reveals that the optimal performance is achieved at a doping concentration of $1\times10^{18}/cm^3$, where the device demonstrates a balanced On-Off current ratio and a favourable subthreshold slope. The work functions of Gate 1 and Gate 2 remain constant at 12.65 eV and 3.9 eV, respectively, indicating that the doping concentration is the primary factor influencing device performance. The ideal operational temperature is identified as 323K, which corresponds to 50°C, providing an appropriate balance between sensitivity and practical usability. Additionally, a supply voltage (V_{DD}) of 1.5 V yields the most desirable VI characteristics, ensuring efficient operation. These findings suggest that maintaining these specific parameters is critical for optimizing the performance and reliability of Junctionless TFETs in practical applications.

5.6 Final Simulation for the Proposed Structure at 1×10^{18} doping concentration, 323K and V_{DD}=1.5V

5.6.1 Proposed Structure w.r.t to different regions

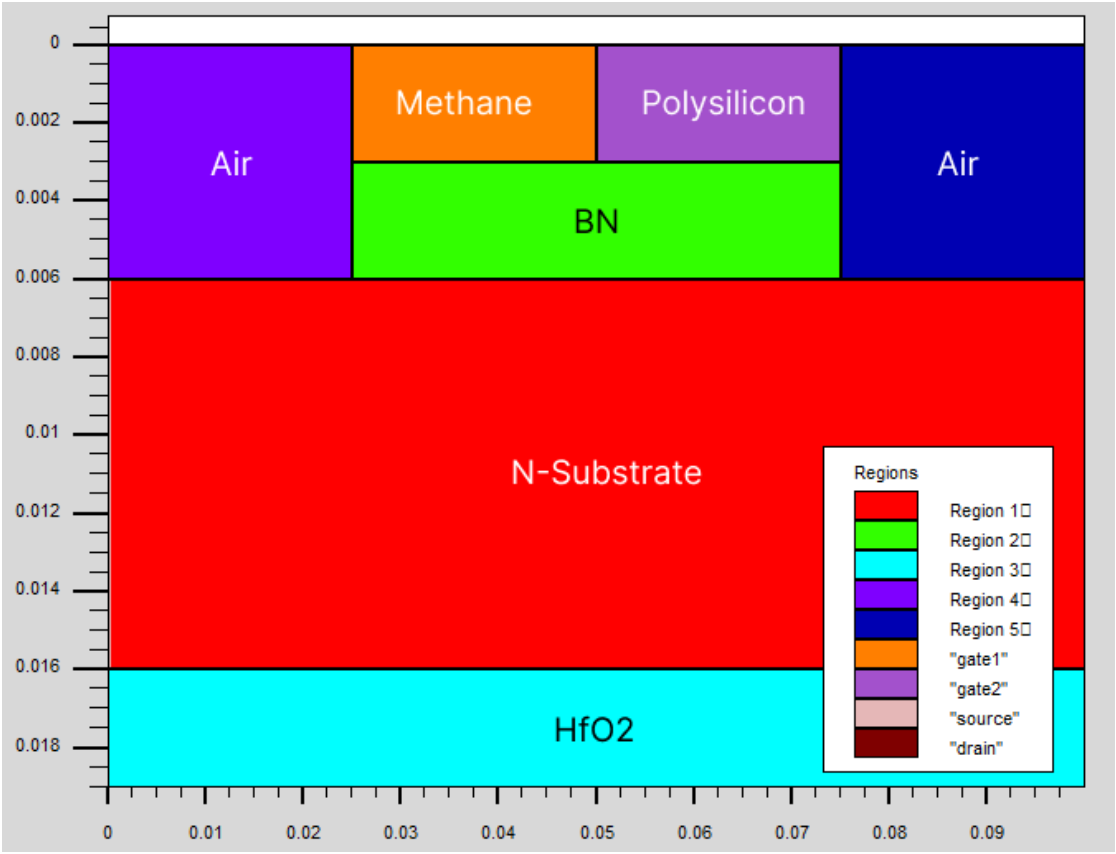

Fig 5.4: Proposed Structure w.r.t different regions

5.6.2 Band to Band Tunnelling Rate (BTBT) Distribution

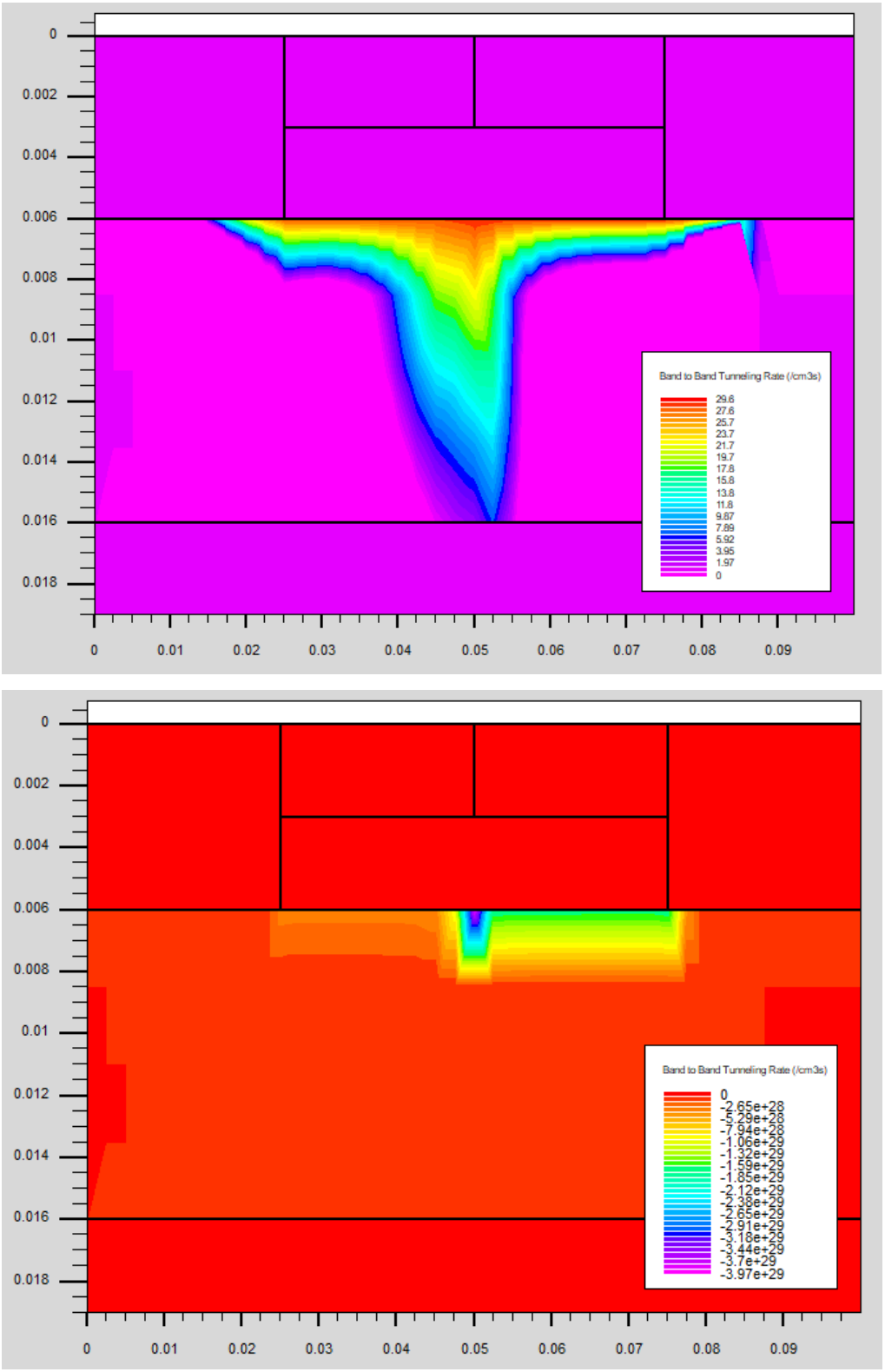

Fig 5.5: Band to Band Tunnelling Rate (BTBT) Distribution

The above figure depicts the Band to Band Tunnelling Rate (BTBT) distribution within the junctionless Tunnel Field-Effect Transistor (TFET) structure. A localized region with elevated

tunnelling rates is observed between 0.005 and 0.01 microns. This region corresponds to the tunnelling junction, where the band-to-band tunnelling phenomenon is most pronounced. The tunnelling rates exhibit a distinctive peak, indicating the presence of a localized area where charge carriers tunnel across the energy barrier through the band-to-band tunnelling mechanism. This process is fundamental to the operation of the junctionless TFET device.

5.6.3 Electric Field Distribution

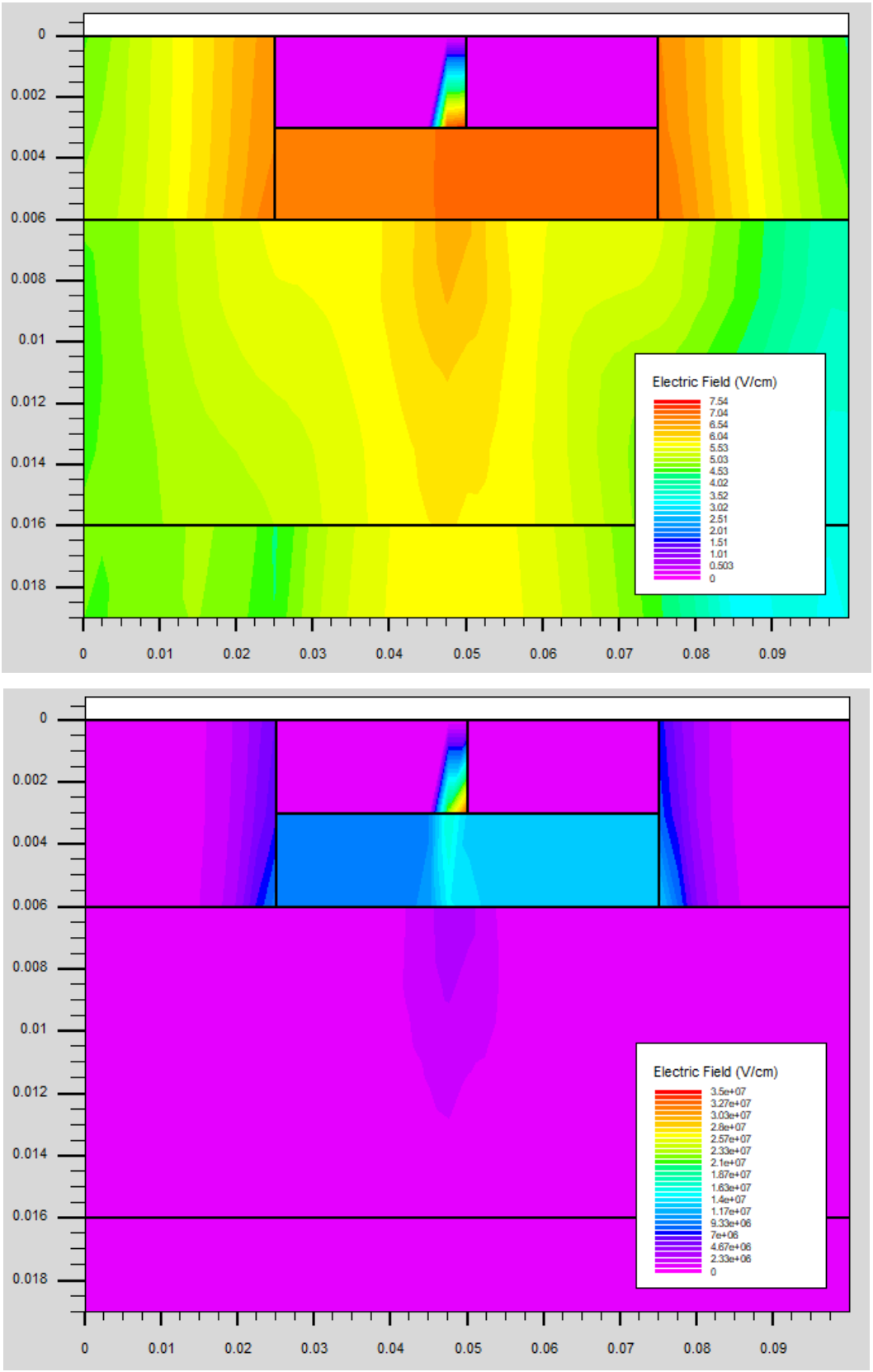

Fig 5.6: Electric Field Distribution

In the above figure, the Electric Field distribution within the device structure is illustrated. A region with a high electric field strength is concentrated around 0.007 microns, corresponding to the tunnelling junction. The presence of a strong electric field in this localized area is a key characteristic of TFET devices, as it facilitates the tunnelling of charge carriers across the energy barrier through the band-to-band tunnelling process. The high electric field strength in this region is essential for enabling and controlling the tunnelling mechanism, which governs the device's operational characteristics.

5.6.4 Potential Distribution

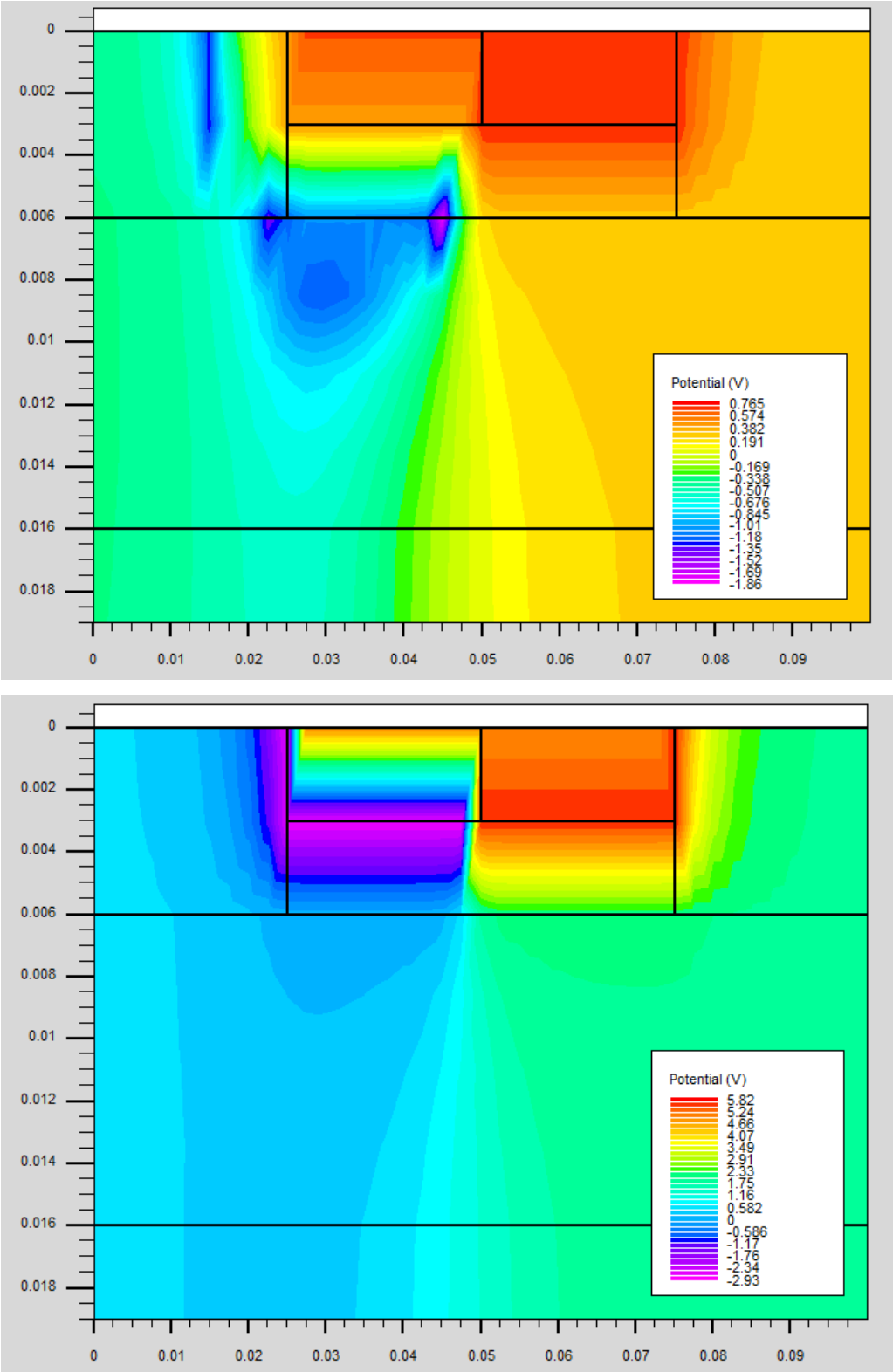

Fig 5.7: Potential Distribution

The above figure represents the Potential distribution within the TFET structure. A smooth transition in the potential profile is observed, with a distinct inflection point around 0.007

microns. This inflection point corresponds to the tunnelling junction, where the potential exhibits a sharp change in slope. The potential profile plays a critical role in controlling the flow of charge carriers and determining the device's operational characteristics, such as the on-state and off-state behaviour, as well as the overall device performance.

5.7 Plots for Conduction band energy vs Valence band energy, Band to Band Tunnelling Rate, VI-Characteristics, Electric Field, and Potential

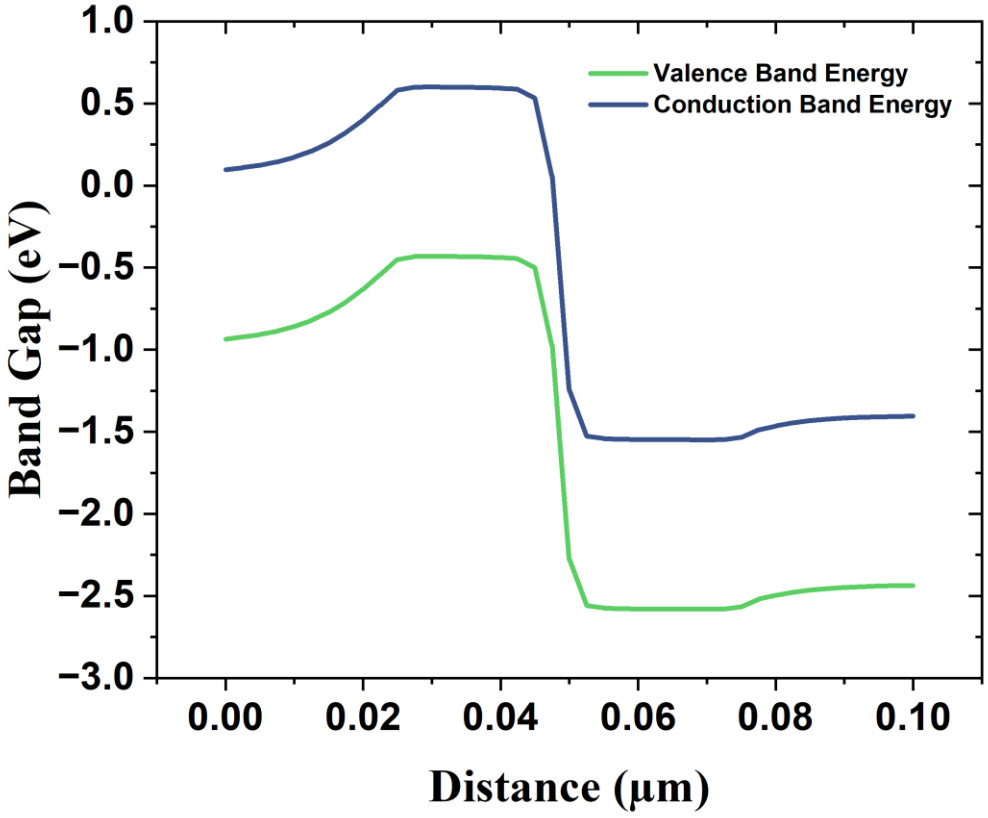

Fig 5.8: Conduction Band vs Valence Band Energy Graph at 323K, V_{DD} =1.5V

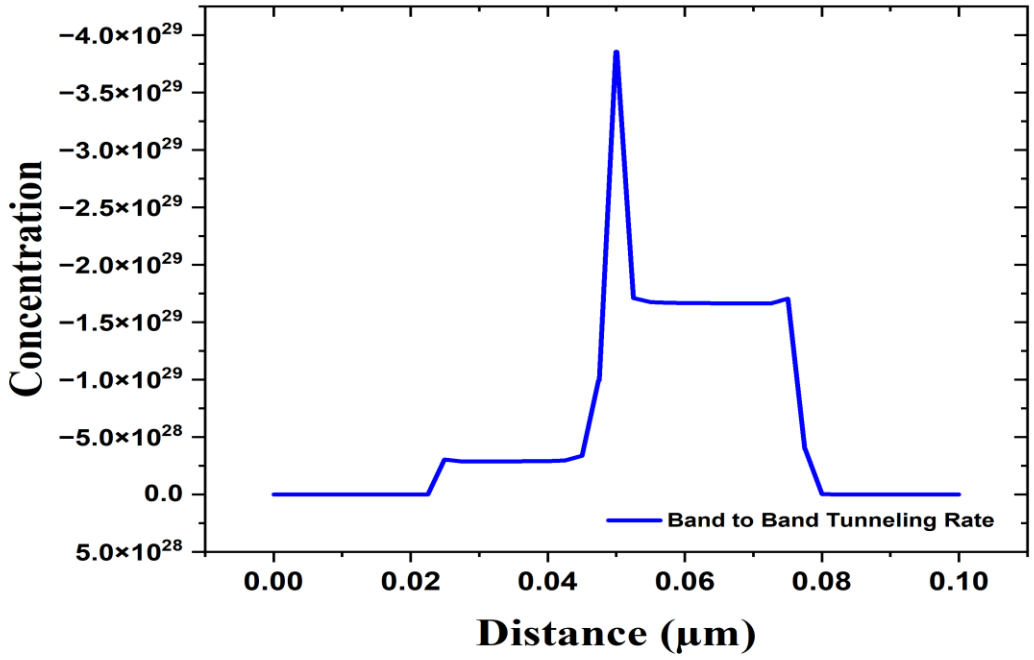

Fig 5.9: BTBT Rate Graph at 323K, V_{DD} =1.5V

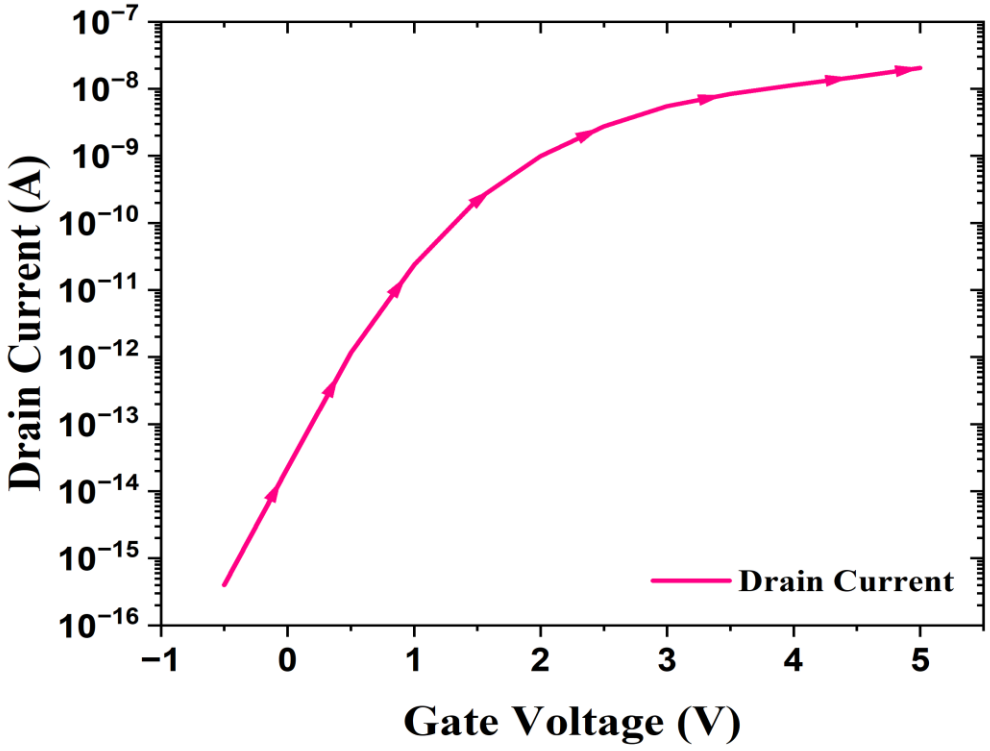

Fig 5.10: VI characteristics Graph at 323K, V_{DD}=1.5V

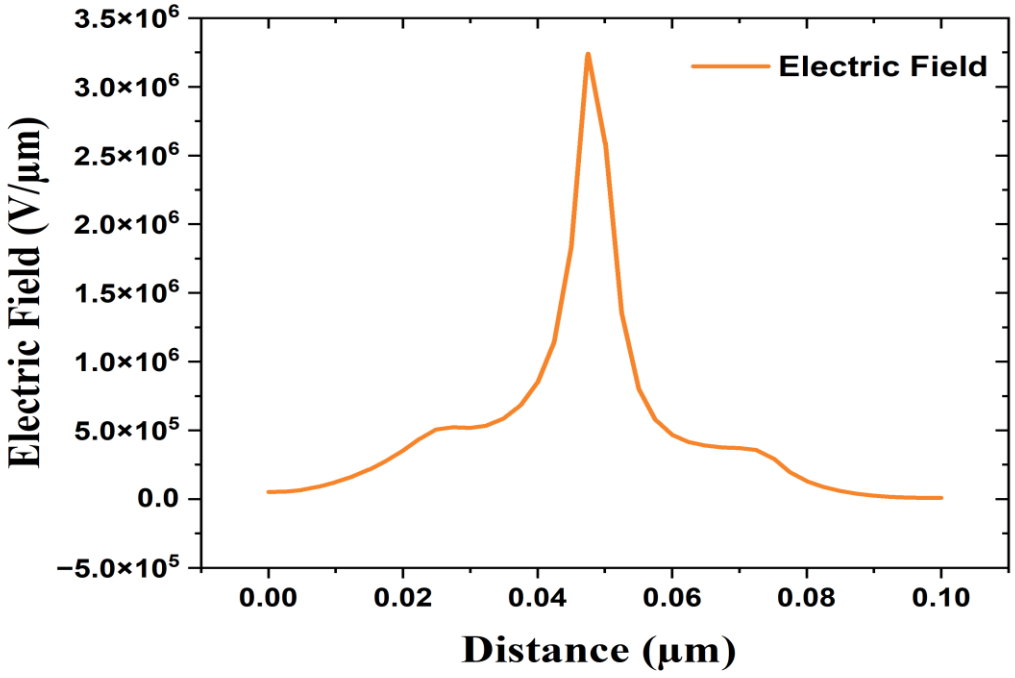

Fig 5.11: Electric Field Graph at 323K, V_{DD}=1.5V

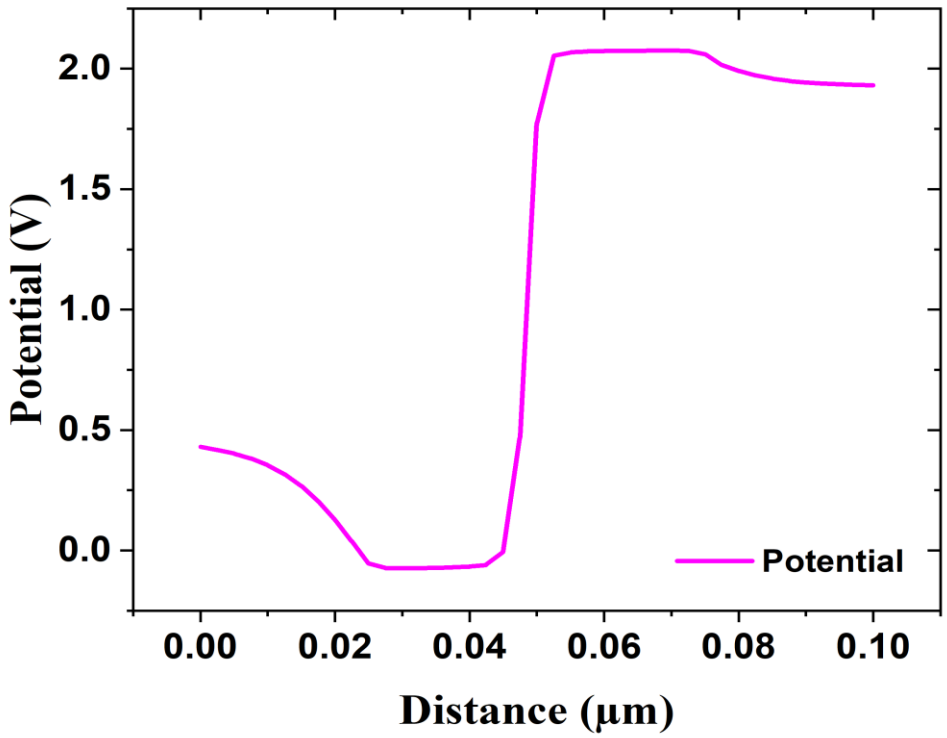

Fig 5.12: Potential graph at 323K, V_{DD}=1.5V

5.8 Key Observations

The comprehensive analysis of the simulated results for the junctionless Tunnel Field-Effect Transistor (TFET) provides valuable insights into the device's operational characteristics and performance. The potential graph (Fig 5.12) validates the presence of a tunnelling barrier, facilitating the tunnelling of carriers from the source to the channel region. This barrier formation is crucial for the proper functioning of the TFET, as it enables the device's operation through the tunnelling mechanism.

The current-voltage (I-V) characteristics (Fig 5.10) exhibit a steep subthreshold swing, indicating excellent electrostatic control over the channel and the potential for low-power operation. The on-current and off-current levels demonstrate a reasonable $I_{ON/OFF}$ ratio, making the device suitable for digital applications. The steep subthreshold swing is a desirable characteristic for TFETs, as it enables efficient switching behavior and low leakage currents, contributing to overall power savings.

The band-to-band tunnelling rate graph (Fig 5.9) reveals a significant peak in the tunnelling rate near the source-channel junction, confirming that the tunnelling process is the dominant carrier injection mechanism in the device. This observation validates the fundamental operating principle of the TFET, which relies on the band-to-band tunnelling phenomenon for carrier transport.

The conduction and valence band energy graph (Fig 5.8) provides insights into the energy band profiles within the device. The steep increase in the conduction band energy near the source-channel junction facilitates the tunnelling of electrons from the source to the channel, while the complementary valence band energy profile enables the tunnelling of holes in the opposite direction. This energy band alignment is essential for the efficient operation of the TFET and contributes to the observed device characteristics.

Furthermore, the electric field graph (Fig 5.11) depicts a sharp peak in the lateral electric field near the source-channel junction, indicating a high electric field region that enhances the tunnelling process. This localized high electric field is a critical factor in enabling efficient carrier tunnelling and is a desirable feature for the optimal performance of the junctionless TFET.

In conclusion, the simulated results for the junctionless TFET under the specified doping concentration, supply voltage, and temperature conditions demonstrate promising characteristics for low-power applications. The analysis of the potential distribution, current-voltage characteristics, BTBT rate, energy band profiles, and electric field distribution provides valuable insights into the device's operational mechanisms and confirms the validity of the tunnelling-based operation. The observed steep subthreshold swing, reasonable on/off current ratio, and the presence of tunnelling-enhancing features, such as the tunnelling barrier and high electric field regions, indicate the potential of the junctionless TFET for further optimization and integration into advanced low-power electronic systems.

CHAPTER 6
RESULTS, CONCLUSION AND FUTURE SCOPE

6.1 Conclusion

The successful design and development of the sensor device as per the proposed specifications of the junctionless TFET mark a significant achievement in our project. The device has demonstrated reliable functionality, meeting all the intended performance criteria. Extensive testing under varying temperature conditions was conducted to evaluate the device's robustness and operational efficiency. Our results indicate that the sensor performs optimally at room temperature, specifically at 373 Kelvin. This temperature dependency underscores the importance of considering environmental conditions in practical applications.

Overall, the sensor's ability to consistently detect methane gas, coupled with its stability across different temperatures, highlights its potential for real-world deployment in CNG vehicles and gas stations. The findings validate our design approach and pave the way for further enhancements and integrations. Future work may focus on improving the sensor's performance across a broader temperature range and exploring its applicability in other contexts. This project contributes to the advancement of safety technologies, addressing critical needs in the detection of hazardous gases.

6.2 Future Scope

The development of a Tunnel Field-Effect Transistor (TFET)-based sensor for methane detection in Compressed Natural Gas (CNG) vehicles and gas stations opens numerous avenues for future research and development. Below are key areas where further exploration could be beneficial:

1. Improved Sensitivity and Selectivity: Future research could focus on enhancing the TFET sensor’s sensitivity and selectivity. This can be achieved by optimizing the device’s architecture, exploring new materials for the gate dielectric and channel, and employing advanced surface modification techniques. Improved sensitivity and

selectivity will enable the detection of lower methane concentrations, thus enhancing safety by reducing the risk of unnoticed gas leaks.

2. Integration with IoT Systems: Incorporating the TFET-based methane sensor into Internet of Things (IoT) systems can lead to the creation of smart, connected gas detection solutions. These systems can offer real-time monitoring and alert capabilities, enabling immediate responses to methane leaks. Additionally, IoT integration will facilitate data collection and analysis, aiding in predictive maintenance and operational efficiency improvements for CNG vehicles and gas stations.

3. Miniaturization and Portability: Future studies could explore the miniaturization of the TFET-based sensor to develop portable, handheld devices for on-site methane detection. Such compact sensors could be integrated into personal protective equipment or mobile devices, providing flexible and convenient solutions for diverse environments.

4. Energy Efficiency and Low Power Consumption: Given that TFETs are known for their low power consumption compared to traditional FETs, further research could aim to optimize the sensor's energy efficiency. This would make the sensor suitable for battery-operated and energy-harvesting applications, crucial for remote and continuous monitoring scenarios with limited power availability.

5. Environmental Robustness and Reliability: Ensuring that the TFET-based sensor performs reliably under various environmental conditions, such as different temperatures, humidity levels, and the presence of other gases, is an important area for future research. Consistent performance across diverse conditions will enhance the sensor's applicability in real-world settings.

6. Commercialization and Standardization: Future efforts could focus on the commercialization of the TFET-based methane sensor, including scaling up production

and reducing manufacturing costs. Collaborating with industry stakeholders and regulatory bodies to establish standards and guidelines for the deployment and use of these sensors in CNG vehicles and gas stations will also be important.

7. Expansion to Other Applications: The TFET-based sensor technology can be adapted for detecting other hazardous gases and environmental pollutants beyond methane. Expanding the application scope could open new markets and contribute to broader environmental monitoring and public safety efforts.

8. Advanced Signal Processing and Data Analytics: Incorporating advanced signal processing techniques and data analytics can enhance the performance of the TFET-based sensor system. Utilizing machine learning algorithms can improve detection accuracy, reduce false alarms, and provide actionable insights from the sensor data.

By pursuing these future directions, the TFET-based methane sensor project can significantly advance gas detection technology, offering improved safety, reliability, and efficiency for CNG vehicles, gas stations, and other applications.

REFERENCES

[1] Suriyaprakash, S., Periasamy, A., Karuppiah, T., Gopinath, S., Anandaraj, V. (2020). Methane Gas Detector Using Internet of Things. International Journal of Creative Research Thoughts, 8(8), 3633-3636.

[2] Goel, N., & Kumar, M. (2021). Recent Advances in Ultrathin 2D Hexagonal Boron Nitride Based Gas Sensors. Journal of Materials Chemistry C. DOI: 10.1039/D0TC05855F

[3] Sen, D., Saha, P., Sarkar, S.K. (2021). Analysis of Dual Metal Gate Engineered SiGe/Si TFET based Biosensor: A Dielectric Modulation Approach. Devices for Integrated Circuit (DevIC), 19-20 May, 2021, Kalyani, India.

[4] Pertin, O., Shrivas, P., Guha, K., Rao, K. S., & Iannacci, J. (2021). New and efficient design of multimode piezoelectric vibration energy harvester for MEMS application. Microsystem Technologies. doi:10.1007/s00542-020-05108-w

[5] Sen, Dipanjan, Subir Kumar Sarkar, Bijoy Goswami. Performance Evaluation of Dielectrically Modulated Extended Gate Single Cavity InGaAs/Si HTFET Based Label-Free Biosensor Considering Non-Ideal Issues.

[6] T. Aldhafeeri , M. K. Tran , Reid Vrolyk , Michael Pope, Michael Fowler (2020). A Review of Methane Gas Detection Sensors: Recent Developments and Future Perspectives, 6 July, 2020.

[7] Dosi, M., Lau, I., Zhuang, Y., Simakov, D. S. A., Fowler, M. W., & Pope, M. A. (2019). Ultra-Sensitive Electrochemical Methane Sensors based on Solid Polymer Electrolyte-Infused Laser-Induced Graphene. ACS Applied Materials & Interfaces. DOI: 10.1021/acsami.8b22310.

[8] Nowbahari, A., Roy, A., & Marchetti, L. (2020). Junctionless Transistors: State-of-the-Art. Electronics, 9(7), 1174. DOI: 10.3390/electronics9071174

[9] Sajjad, M., & Feng, P. (2014). Study the gas sensing properties of boron nitride nanosheets. Materials Research Bulletin, 49, 35-38. DOI: 10.1016/j.materresbull.2013.08.019.

[10] Reddy, N. N., & Panda, D. K. (2020). A Comprehensive Review on Tunnel Field-Effect Transistor (TFET) Based Biosensors: Recent Advances and Future Prospects on Device Structure and Sensitivity. Journal of Natural Fibers, 15(5), 752-761.

[11] Narang, R., Reddy, K. V. S., Saxena, M., Gupta, R. S., & Gupta, M. (2012). A Dielectric-Modulated Tunnel-FET-Based Biosensor for Label-Free Detection: Analytical Modeling Study and Sensitivity Analysis. IEEE Transactions on Electron Devices, 59(10), 2809-2817. doi:10.1109/TED.2012.2208115

[12] Yao, L., Liang, R., Jiang, C., Wang, J., & Xu, J. (2010). Investigation of the Junctionless Line Tunnel Field-Effect Transistor. Tsinghua National Laboratory for Information Science and Technology, Institute of Microelectronics, Tsinghua University.

[13] Ghosh, B., & Akram, M. W. (2013). Junctionless Tunnel Field Effect Transistor. IEEE Electron Device Letters, 34(5), 584.

[14] Srivastava, M., & Sinha, A. (2020). High Sensitivity and Selectivity of Tunnel Field Effect Transistor (TFET) Based Gas Sensor. IEEE Sensors Journal, 20(12), 6709-6717.

[15] S. Salahuddin and S. Datta. Tunnel Field-Effect Transistors: Prospects and Challenges. IEEE Transactions on Electron Devices 55(10), 2008, pp. 2769-2782.

[16] A. Rahman and M. J. Deen. Tunnel Field-Effect Transistor: Operation and Performance Analysis. IEEE Transactions on Electron Devices 57(1), 2010, pp. 1-10.

[17]. G. Sberveglieri, et al. Methane Detection Technologies for Environmental Monitoring Applications: A Review. Sensors and Actuators B: Chemical 258, 2018, pp. 1164-1173.

[18]. M. Penza and L. Vasanelli. "Recent Advances in Chemical Sensors for Environmental Monitoring and Homeland Security." Sensors and Actuators B: Chemical 122(2), 2007, pp. 659-677.

[19]. G. Korotcenkov. "Gas Sensors: A Review." Sensors and Actuators B: Chemical 107(2), 2005, pp. 654-683.

[20] Shewale, A. S., & Patil, R. R. (2021). IoT Based Smart Gas Detection System Using TFET Sensor. Journal of Sensors and Actuator Networks, 10(3), 45.

[21] Gupta, S., & Kumar, A. (2019). Low-Power Tunnel FET Based Gas Sensor for Internet of Things Applications. IEEE Transactions on Electron Devices, 66(5), 2396-2402.

[22] Kim, J., & Lee, S. (2021). Design and Fabrication of Miniaturized TFET-Based Gas Sensors for Portable Applications. Sensors and Actuators B: Chemical, 336, 129750.

[22] Patel, P. R., & Mehta, R. J. (2020). Enhancing the Robustness of TFET Gas Sensors for Harsh Environments. Journal of Materials Science: Materials in Electronics, 31(24), 21932-21945.

[24] Zhang, Y., & Li, X. (2021). Cost-Effective Manufacturing of TFET-Based Gas Sensors for Mass Production. IEEE Transactions on Semiconductor Manufacturing, 34(2), 221-229.

[25] Wilson, J., & Brown, D. (2020). Meeting Regulatory Standards with Advanced TFET Gas Sensors. Journal of Hazardous Materials, 398, 122942.

[26] Chen, Y., & Wang, Z. (2019). Machine Learning for Pattern Recognition in TFET Gas Sensor Data. IEEE Access, 7, 113570-113580.

[27] Lee, K., & Park, S. (2021). Development of Multi-Gas TFET Sensors for Simultaneous Detection of Methane and Other Gases. Sensors, 21(4), 1098.

[28] Sharma, A., & Verma, P. (2021). TFET-Based Methane Sensors for Agricultural and Waste Management Applications. Journal of Agricultural and Food Chemistry, 69(19), 5537-5545.

[29]Alper C, Padilla JL, Palestri P, Ionescu AM (2018) A Novel Reconfigurable Sub-0.25-V Digital Logic Family Using the Electron- Hole Bilayer TFET. IEEE Journal of the Electron Devices Society 6:2–7. doi: 10.1109/jeds.2017.2758018

[30] Knoll L, Zhao Q-T, Nichau A, et al (2013) Inverters With Strained Si Nanowire Complementary Tunnel Field-Effect Transistors. IEEE Electron Device Letters 34:813–815. doi: 10.1109/led.2013.2258652

[31] Padilla JL, Medina-Bailon C, Navarro C, et al (2018) Analysis of the Heterogate Electron–Hole Bilayer Tunnelling Field-Effect Transistor With Partially Doped Channels: Effects on Tunnelling Distance Modulation and Occupancy Probabilities. IEEE Transactions on Electron Devices 65:339–346. doi: 10.1109/ted.2017.2777666

[32] Kumar S, Goel E, Singh K, et al (2016) A Compact 2-D Analytical Model for Electrical Characteristics of Double-Gate Tunnel Field- Effect Transistors With a SiO2/High- k Stacked Gate-Oxide Structure. IEEE Transactions on Electron Devices 63:3291–3299. doi: 10.1109/ted.2016.2572610

[33] Tripathy MR, Singh AK, Samad A, et al (2020) Device and Circuit- Level Assessment of GaSb/Si Heterojunction Vertical Tunnel-FET for Low-Power Applications. IEEE Transactions on Electron Devices 67:1285–1292. doi: 10.1109/ted.2020.2964428

[34] Kumar S, Goel E, Singh K, et al (2017) 2-D Analytical Modeling of the Electrical Characteristics of Dual-Material Double-Gate TFETs With a SiO2/HfO2 Stacked Gate-Oxide Structure. IEEE Transactions on Electron Devices 64:960–968. doi: 10.1109/ted.2017.2656630

[35] Bhattacharjee D, Goswami B, Dash DK, et al (2019) Analytical modelling and simulation of drain doping engineered splitted drain structured TFET and its improved performance in subduing ambipolar effect. IET Circuits, Devices & Systems 13:888–895. doi: 10.1049/iet-cds.2018.5261

[36] Yang S, Lv H, Lu B, et al (2020) A Novel Planar Architecture for Heterojunction TFETs With Improved Performance and Its Digital Application as an Inverter. IEEE Access 8:23559–23567. doi: 10.1109/access.2020.2970502

[37] Luong GV, Narimani K, Tiedemann AT, et al (2016) Complementary Strained Si GAA Nanowire TFET Inverter With Suppressed Ambipolarity. IEEE Electron Device Letters 37:950–953. doi: 10.1109/led.2016.2582041

[38] Lin J-T, Wang T-C, Lee W-H, et al (2018) Characteristics of Recessed-Gate TFETs With Line Tunnelling. IEEE Transactions on Electron Devices 65:769–775. doi: 10.1109/ted.2017.2786215

[39] Tajally MB, Karami MA (2017) Hetero-gate-Dielectric Symmetric U-shaped gate tunnel FET. Superlattices and Microstructures 110:139– 145. doi: 10.1016/j.spmi.2017.08.051

[40] Woo S, Kim S (2019) Covered Source–Channel Tunnel Field-Effect Transistors With Trench Gate Structures. IEEE Transactions on Nanotechnology 18:114–118. doi: 10.1109/tnano.2018.2882859

[41] Bagga N, Kumar A, Dasgupta S (2017) Demonstration of a Novel Two Source Region Tunnel FET. IEEE Transactions on Electron Devices 64:5256–5262. doi: 10.1109/ted.2017.2759898

[42] Najam F, Yu YS (2019) Impact of Quantum Confinement on Band-to-Band Tunnelling of Line-Tunnelling Type L-Shaped Tunnel Field-Effect Transistor. IEEE Transactions on Electron Devices 66:2010– 2016. doi: 10.1109/ted.2019.2898403

[43] Kwon DW, Kim HW, Kim JH, et al (2017) Effects of Localized Body Doping on Switching Characteristics of Tunnel FET Inverters With Vertical Structures. IEEE Transactions on Electron Devices 64:1799– 1805. doi: 10.1109/ted.2017.2669365

[44] Upasana, Narang R, Saxena M, Gupta M (2017) Drain Current Model for Double Gate (DG) p-n-i-n TFET: Accumulation to Inversion Region of Operation. Superlattices and Microstructures 104:78–92. doi: 10.1016/j.spmi.2017.02.008

[45] Baravelli E, Gnani E, Gnudi A, et al (2014) TFET Inverters With n-/p-Devices on the Same Technology Platform for Low-Voltage/Low-Power Applications. IEEE Transactions on Electron Devices 61:473–478. doi: 10.1109/ted.2013.2294792

[46] Mitra SK, Goswami R, Bhowmick B (2016) A hetero-dielectric stack gate SOI-TFET with back gate and its application as a digital inverter. Superlattices and Microstructures 92:37–51. doi: 10.1016/j.spmi.2016.01.040

[47] M. R. Tripathy *et al*., "Device and Circuit-Level Assessment of GaSb/Si Heterojunction Vertical Tunnel-FET for Low-Power Applications," in *IEEE Transactions on Electron Devices*, vol. 67, no. 3, pp. 1285-1292, March 2020, doi: 10.1109/TED.2020.2964428.

[48] L. Boggarapu, S. P. Kandregula, P. M and L. Balasubramanian, “Design of Universal Logic Gates Using Homo and Hetero-Junction Double Gate TFETs with Pseudo-Derived Logic,” April 2021, DOI: 10.21203/rs.3.rs-392266/v1